Summer 2009

EMI failure analysis techniques and noise prediction for trace crossing split planes

Weifeng Pan

EMI FAILURE ANALYSIS TECHNIQUES

AND

NOISE PREDICTION FOR TRACE CROSSING SPLIT PLANES

by

WEIFENG PAN

A DISSERTATION

Presented to the Faculty of the Graduate School of the

MISSOURI UNIVERSITY OF SCIENCE & TECHNOLOGY

In Partial Fulfillment of the Requirements for the Degree

DOCTOR OF PHILOSOPHY

in

ELECTRICAL ENGINEERING

2009

Approved by

David J. Pommerenke, Advisor
James L. Drewniak
Richard E. DuBroff
Daryl G. Beetner
Matthew J. O'Keefe

PUBLICATION DISSERTATION OPTION

This dissertation has been prepared in four papers for publication formatted in the style used by the Missouri University of Science and Technology. The first three papers have been submitted for publication in the IEEE Electromagnetic Compatibility Society Newsletters. The fourth paper will be submitted for publication in the IEEE Transactions on Electromagnetic Compatibility.

ABSTRACT

A variety of methods exist that help locate the source, coupling path, and antenna in an electromagnetic interference (EMI) problem. No single method is the best option in all cases. A good electromagnetic compatibility (EMC) engineer should understand and have experience with a wide range of failure analysis methods and thus, be able to select the most appropriate ones for a given problem. The first three papers are from a series of articles, which explains a set of methods for the analysis of EMI failures. Each method is categorized based on two criteria: 1) the elements in an EMI problem each method tries to determine: the source, coupling path or the antenna; 2) the complexity of each method. The methods are explained to guide EMC engineers in selecting the right one by evaluating the advantages and limitations of each method.

Printed circuit boards (PCBs) often have high speed data traces crossing splits in the adjacent reference planes due to space limitations and cost constraints. These split planes usually result from different power islands on nearby layers. The fourth paper quantifies the effects of the split planes and the associated stitching capacitors for various stack-up configurations.

ACKNOWLEDGMENTS

First, my sincere gratitude and respect go to Dr. David Pommerenke and Dr. James Drewniak. The knowledge and the professionalism they have taught me, and the help they have offered to me with my work and life, will continue to be enduring and encouraging in my career.

Dr. Richard DuBroff proofread this dissertation and provided with me many valuable advices.

I would also like to express my thankfulness to Dr. Daryl Beetner, Dr. Matthew J. O'Keefe, and Dr. Jun Fan, for their help and guidance on my research and Ph.D. dissertation.

Finally, I would like to express my appreciation to all the colleagues and students in the UMR/MST EMC Lab for their team work and help in aspects of this research.

TABLE OF CONTENTS

Page

PUBLICATION DISSERTATION OPTION iii

ABSTRACT iv

ACKNOWLEDGMENTS v

LIST OF ILLUSTRATIONS viii

LIST OF TABLES x

PAPER

1. EMI FAILURE ANALYSIS TECHNIQUES: I. FREQUENCY SPECTRUM ANALYSIS 1

1.1. INTRODUCTION 1

1.2. BROADBAND SPECTRUM MEASUREMENT 5

1.3. NARROW SPECTRUM MEASUREMENT 7

1.4. ZERO SPAN MEASUREMENT 13

1.5. CONCLUSION 15

REFERENCES 15

2. EMI FAILURE ANALYSIS: II. JOINT TIME-FREQUENCY ANALYSIS 16

2.1. INTRODUCTION 16

2.2. APPLICATIONS OF STFFT 18

2.3. SUMMARY 21

2.4. CONCLUSION 24

REFERENCES 24

3. EMI FAILURE ANALYSIS TECHNIQUES: III. CORRELATION ANALYSIS 26

3.1. INTRODUCTION 26

3.2. MATHEMATICAL CORRELATION METHODS 26

3.2.1. STFFT Correlation. 28

3.2.2. Envelope Correlation. 29

3.2.3. Coherence Factor. 32

3.2.4. Direct Correlation. 34

3.2.5. Amplitude Density Distribution. 34

3.3. CONCLUSION 36
REFERENCES 38
4. PREDICTING NOISE VOLTAGE FROM TRACE CROSSING SPLIT PLANES ON PRINTED CIRCUIT BOARDS 39
4.1. ABSTRACT 39
4.2. INTRODUCTION 40
4.3. MICROSTRIP CONFIGURATION 44
4.4. STRIPLINE CROSSING SPLIT PLANES 50
4.5. MEASUREMENT VALIDATION 51
4.6. CONCLUSION 53
REFERENCES 54
CONCLUSIONS 56
VITA 57

LIST OF ILLUSTRATIONS

Page

Figure 1.1. Typical far-field broadband measurement setup. 6

Figure 1.2. Far-field radiation measurement on three TVs. 7

Figure 1.3. Narrowband measurement of the far-field radiation at 125 MHz from a mother board. 9

Figure 1.4. Super narrowband scan of the far-field signal from an EUT. 9

Figure 1.5. Far-field before and after modification at 72 MHz. 11

Figure 1.6. Far-field before and after a modification at 252 MHz. 12

Figure 1.7. Two sources distinguished by the sidebands pattern have different antenna structures, thus different radiation patterns. 12

Figure 1.8. Far-field spectrum around 288 MHz for two turn-table positions. 13

Figure 1.9. Zero span measurement (RBW = 10 MHz) of the signal in Figure 1.2 at 270 MHz. 14

Figure 2.1. Basic STFFT process. 17

Figure 2.2. Narrowband spectrum at 931 MHz of a far-field signal. 19

Figure 2.3. STFFT result zoomed in to 840 ~ 960 MHz, showing the dithered clock. 19

Figure 2.4. EMI of a switched power supply. 20

Figure 2.5. Strong 280 MHz centered broadband emissions shown in the STFFT domain (top) and associated voltage (bottom) in the buck converter. 22

Figure 2.6. Typical circuit diagram of a synchronous DC-DC buck converter. 22

Figure 3.1. Time-synchronized measurement of far-field and near-field for correlation analysis. 27

Figure 3.2. STFFT spectrograms (1st and 3rd plots) and time domain waveforms (2nd and 4th plots) of near-field and far-field signals. 30

Figure 3.3. Envelope at 667 MHz of a near-field signal and the far-field. 32

Figure 3.4. Coherence factor between a near-field signal and the far-field signal. 33

Figure 3.5. Direct correlation of a near-field signal and the far-field. 35

Figure 3.6. Comparing the amplitude density distribution of far-field and a near-field signal. 37

Figure 3.7. Amplitude density distribution of the far-field and from a signal captured by current clamp. 37

Figure 4.1. A depiction of the current flow for a microstrip crossing split planes. 42

Figure 4.2. Equivalent circuit model of the case in Figure 4.1. 42

Figure 4.3. Transmission line model of microstrip crossing a slot. 43

Figure 4.4. Simulation structure of a microstrip crossing split plane, top and cross section view. 46

Figure 4.5. Simulation result: voltage waveforms of source and at all the voltage probes. 47

Figure 4.6. Impedance by normalizing maximum voltage across split to current on trace. 48

Figure 4.7. Equivalent inductance calculated using the impedance in Figure 4.6. 49

Figure 4.8. Simulation and curve fitting for low frequency part of the equivalent inductance. 49

Figure 4.9. Simulation structure of a stripline across split, cross section view. 50

Figure 4.10. Simulation and curve fitting for low frequency part of the equivalent inductance. 52

Figure 4.11. Test board with microstrip crossing split. 52

Figure 4.12. Validation between simulation data and measurement result of the test board. 53

LIST OF TABLES

Page

Table 1.1. Overview of the EMI analysis techniques. 2
Table 2.1. Suggested measurement sequence for EMI source identification. 23
Table 3.1. Overview of the correlation methods..... 28
Table 4.1. Combination of values of $h_1$and h_2 used in simulation. 50

PAPER

1. EMI FAILURE ANALYSIS TECHNIQUES: I. FREQUENCY SPECTRUM ANALYSIS

Weifeng Pan and David Pommerenke, with contributions from all members of the EMC Laboratory at Missouri University of Science & Technology

1.1. INTRODUCTION

Products fail electromagnetic interference (EMI) tests. This can be a disappointing experience, or it can be part of a design strategy that seeks to implement only the needed countermeasures and thus accepts, or even encourages failures on the initial EMI test. Either way, the reason for the failure must be determined. A variety of methods exist that help locate the source, coupling path, and antenna. No single method is the best option in all cases. A good electromagnetic compatibility (EMC) engineer should understand and have experience with a wide range of failure analysis methods and thus be able to select the most appropriate ones for a given problem.

This series of articles explains a set of methods for the analysis of EMI failures. Each method is categorized based on two criteria: 1) Does the method determine the source, coupling path or the antenna of an EMI problem? 2) Is the method simple, or does it require special equipment and advanced processing? We want to explain methods and guide EMC engineers in selecting the right one by evaluating the advantages and limitations of each method. Table 1.1 provides an overview of the major EMI analysis techniques that have been studied and practiced in our lab.

Table 1.1. Overview of the EMI analysis techniques.

Method		Application	For identifying …	Complexity
Frequency spectrum analysis	Broadband measurement	Obtain an overview of the radiated emission. Distinguish between narrowband and broadband signals.	General	Easy
	Narrowband measurement	Analyze at very narrow span to identify fine spectra details, e.g., sidebands, for distinguishing between possible sources.	Source	Easy
	Zero span measurement	For narrowband signal: differentiate AM or FM modulation. For broadband signal: determine switching frequencies.	Source	Easy
Short term FFT analysis		Reveal how a signal spectrum evolves with time. Identify EMI sources from multiple broadband sources in a complex system.	Source	Complex
Correlation analysis		Analyze mathematical correlation between near-field sources and far-field, or among multiple near-field observations.	Source	Complex

Table 1.1. Overview of the EMI analysis techniques (cont.)

Resonance analysis	Swept frequency measurement	Investigate the resonance behavior by substituting a swept frequency clock for the source.	Coupling path/antenna	Moderate
	Resonance identification	Use manual probing or near-field scanning to locate the resonance on a printed circuit board (PCB) or metal structure.		Moderate
	Resonance scanning	S_{21} scanning for each point on a PCB using a cross probe to find local resonance and coupling path.		Complex
Port voltage and port impedance measurement		Measure between two metal parts on a PCB or enclosure to find suspected antenna structure and noise voltage.	Coupling path/antenna	Easy
Transfer impedance measurement		Quantify coupling path (coupling strength from the source to other structures). Substitute an external signal for a possible EMI source.	Coupling path	Complex
Near-field scanning		Use scanning system to obtain the E or H field distribution across the user-defined area on the equipment under test (EUT).	Source/coupling path	Complex

Table 1.1. Overview of the EMI analysis techniques (cont.)

Current clamp and E/H field probe measurement		Measure common mode current on cables, then estimate far-field. Measure or inject E/H field on EUT.	Source/coupling path	Moderate
TEM cell measurement		Determine the main EMI excitation mechanism: E or H field coupling. The board has 10 cm × 10 cm standard size.	Coupling path	Complex
Small techniques	Obtain radiation pattern using spectrum analyzer	A quick view of the radiation pattern of the EUT.	Antenna	Easy
	Use strong magnet to remove effect of a ferrite	A fast method to remove the effect of ferrite without physically changing the circuit/board structure.	Coupling path	Easy
	Press and observe amplitude change to distinguish contact and proximity effect	Loose contact of metal connectors or proximity of noisy cables to metals may cause bad repeatability of EMI tests. By observing the magnitude in zero span measurement, abrupt changes indicate contact effect, while smooth changes indicate proximity effect.	Coupling path	Easy

In this article, several frequency spectrum analysis strategies are suggested. Often the spectrum is just observed using typical EMI settings: 120 kHz resolution bandwidth (RBW), peak or quasi-peak. However, with very little effort more information can be obtained just using the spectrum analyzer. At first, it is worthwhile to distinguish broadband from narrowband signals. Then zero span analysis is suggested. If an oscilloscope is attached to the antenna, the time evolving sprectrum can be observed and the correlations between near-field probing and far-field can be performed. Some of these analyses could quite easily be implemented in automated software, such that a critical frequency is analyzed further, to give the designer additional information.

1.2. BROADBAND SPECTRUM MEASUREMENT

As a first step in EMI evaluation, an overview is useful of the radiated emission from the EUT in the entire frequency range of interest. Such an overview locates the problematic frequencies in the spectrum and compares their amplitude with the maximum allowed by EMC regulations [1]. A typical far-field measurement setup is shown in Figure 1.1.

A large RBW of 100 kHz ~ 1 MHz is usually used to measure radiated emission from 30 MHz up. To obtain a quick overview, max-hold is used while rotating the turntable and gathering data in both antenna polarizations and at various heights.

A typical result is shown in Figure 1.2, which compares three televisions (TV) of the same model. The broadband signals around 65 and 270 MHz and narrowband signals at about 150 and 490 MHz are relatively strong in comparison with the emission limit.

Differences are apparent among the supposedly identical TVs. What can we learn from these differences? Experience tells us that mass produced electronic boards are very similar, but their mechanical assemblies are more likely to vary. For example, contact between metal parts and routing of cables tend to vary more than the signals on a PCB. Thus, at frequencies where electronic products of the same model show considerable difference, a focus on these mechanical assembly factors can help identify EMI coupling paths.

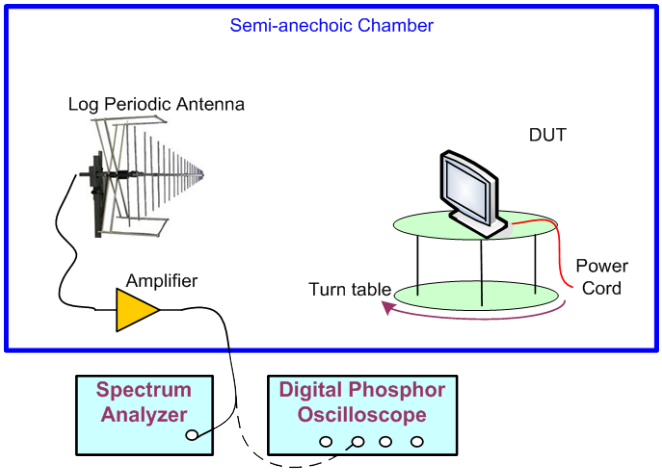

Figure 1.1. Typical far-field broadband measurement setup.

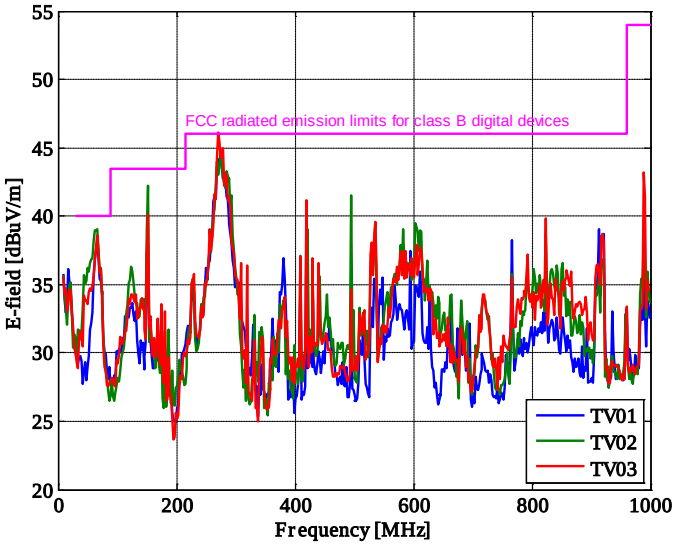

Figure 1.2. Far-field radiation measurement on three TVs.

1.3. NARROW SPECTRUM MEASUREMENT

Analysis of narrowband signals requires looking at the spectrum near the carrier frequency. The objective is to find the EMI source by correlating local signals to the far-field. This correlation is trivial if there is only one semiconductor operating at that frequency; this situation would be nice but it is rare. In most systems, many integrated circuits (IC), or even modules, operate at the same frequency or with the same harmonics. The underlying idea is to identify subtle differences in the near spectrum among signals having the same frequency and then correlate those differences to the far-field spectral signature.

For example, in a phase locked loop (PLL), the reference signal from a crystal oscillator has very low phase noise and no sidebands. But the PLL might add phase noise and side bands. Some noise (e.g., 100 kHz) may be added to the PLL VDD. This will

cause periodic jitter, i.e., sidebands, to the PLL. Those are easy to detect, and in many cases this additional noise will not affect the functionality of the system.

Figure 1.3 shows a narrowband measurement (100 Hz RBW and 6 kHz span) of the far-field radiation at 125 MHz from a mother board. There are two signals very close in frequency: one is from the on-board clock, the other is PLL synthesized from LAN signal. They will otherwise show up as one signal in a broadband measurement.

A data signal and clock signal provide another example. Data signal is more likely to be amplitude modulated whereas clocks are often phase modulated. Power supply variations may modulate the PLL phase at the data frequency, thus data and clock have similar sideband structures, but one is phase modulated and the other is amplitude modulated. Zero-span analysis or I/Q demodulation can differentiate between amplitude and phase modulation, even if the sideband magnitude is the same.

Figure 1.4 shows the far-field signal from an EUT. The EUT has many clocks, but they are all phase locked to an 18 MHz reference. The insert in Figure 1.4 shows the near spectrum and sidebands of the harmonic centered at 144 MHz. Those sidebands are usually visible at kHz or lower span setting. For each harmonic, the measurement software captures not only its amplitude in 120 kHz RBW, but also its sidebands in a span set by the user, providing data for correlation between near-field and far-field.

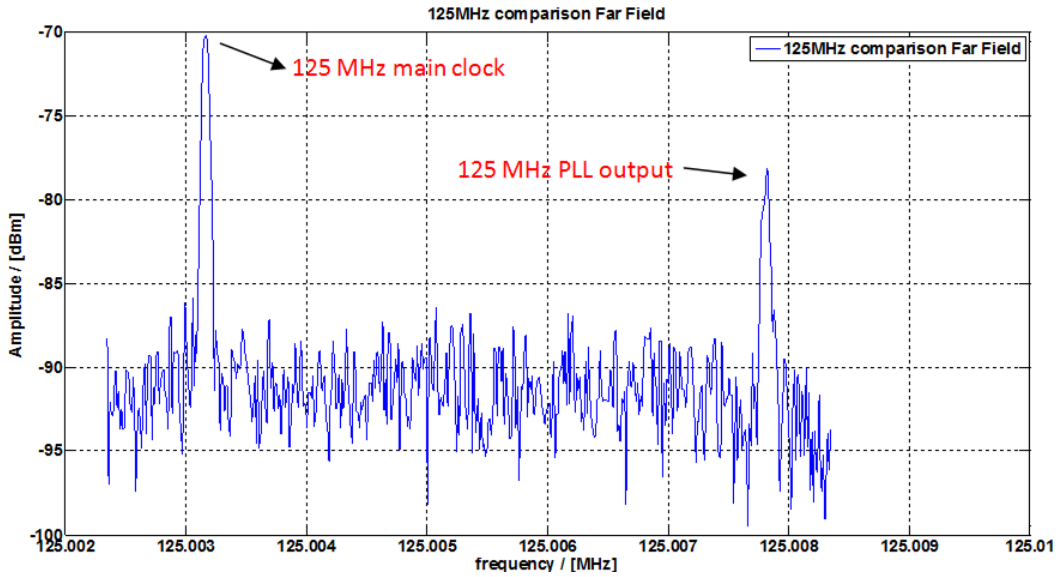

Figure 1.3. Narrowband measurement of the far-field radiation at 125 MHz from a mother board.

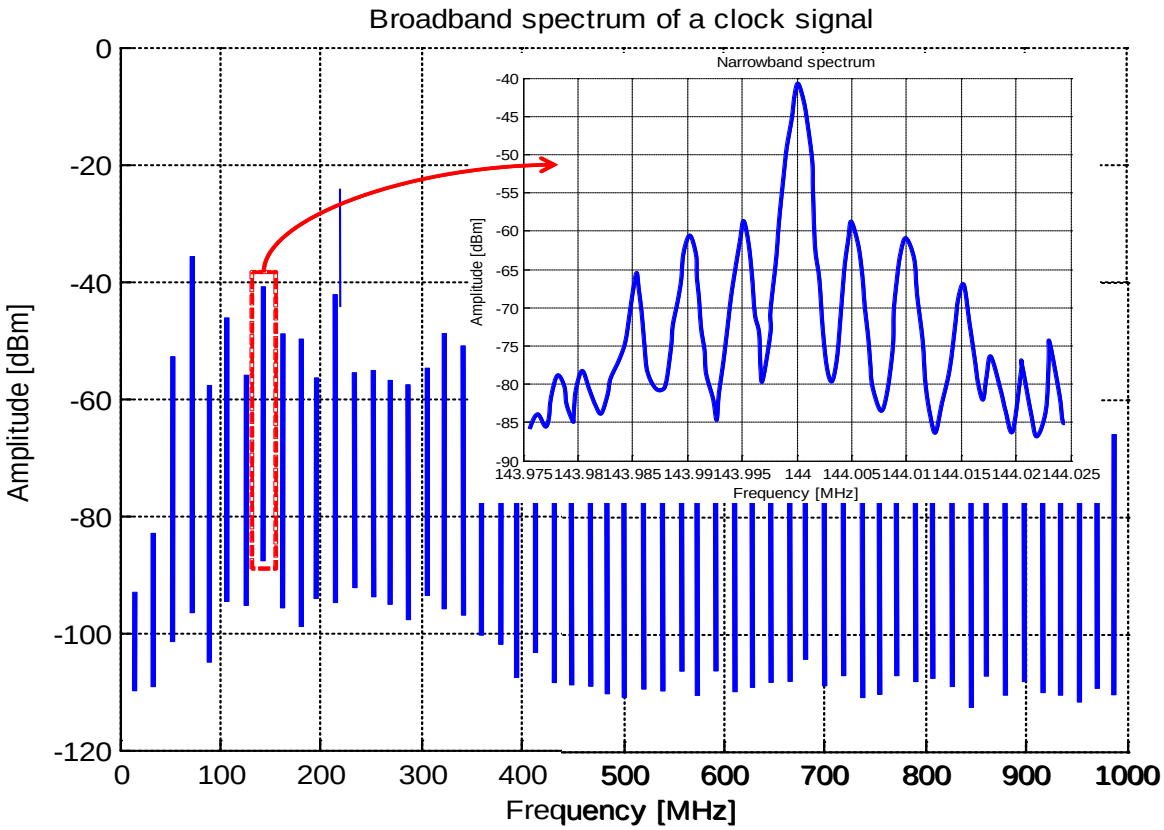

Figure 1.4. Super narrowband scan of the far-field signal from an EUT.

If it is not clear which IC is contributing to the far-field emission, the source can sometimes be identified by correlating the sideband structure of the far-field to the different possible ICs (more advanced correlation techniques for broadband signals will be addressed in a future article in this series). Instead of the far-field, a current clamp is often used to measure cable current that determines the far-field; another option is the voltage across a slot, if this slot is the radiating antenna. The reason for substituting the far-field by a relevant near-field measurement is to avoid field changes caused by person standing around the EUT while probing to find the best correlation.

A really difficult EMI debugging situation occurs when a problematic radiation is caused by more than one antenna and coupling path. In such situations counter-intuitive phenomena can be confusing. For example, shielding a product may create stronger emission! As an example, the EMI antenna receives the vector sum of the signals. If two sources of similar magnitude reach the antenna, they can constructively or destructively interfere. If they interfere destructively and one signal is shielded, the total signal will increase!

When multiple sources transmit at the same frequency but differ in spectral details, the source can still be identified by carefully analyzing the narrowband spectrum of the far-field and comparing it with that of locally measured signals. The case illustrated in Figure 1.4 shows how two potential EMI sources can be differentiated from sideband spectra. If the far-field is dominated by a signal with sidebands, a modification will change both the carrier and the sidebands. This is the case at 72 MHz (Figure 1.5).

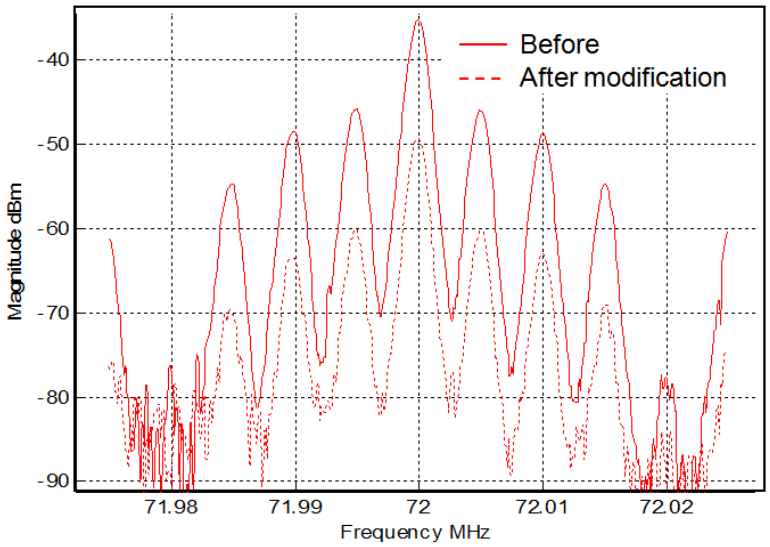

Figure 1.5. Far-field before and after modification at 72 MHz. Main signal and sidebands change by the same amount. The far-field is dominated by the signal with sidebands.

But at 252 MHz the situation is quite different. The signal received by the log-periodic antenna is a superposition of both sources, and the modification affects only the signal without sidebands. We will observe the spectrum shown in Figure 1.6.

If these two signals radiate from different antennas, the two antennas likely have different radiation patterns (Figure 1.7). In such a case, the sideband-to-carrier ratio will be a function of the antenna rotation. In Figure 1.8, the carrier signal is reduced by about 5 dB if the turntable is rotated from 86° to 191° but the sidebands remain at about -70 dB. Two sources, one with sidebands and one without, are emitted from different antenna structures.

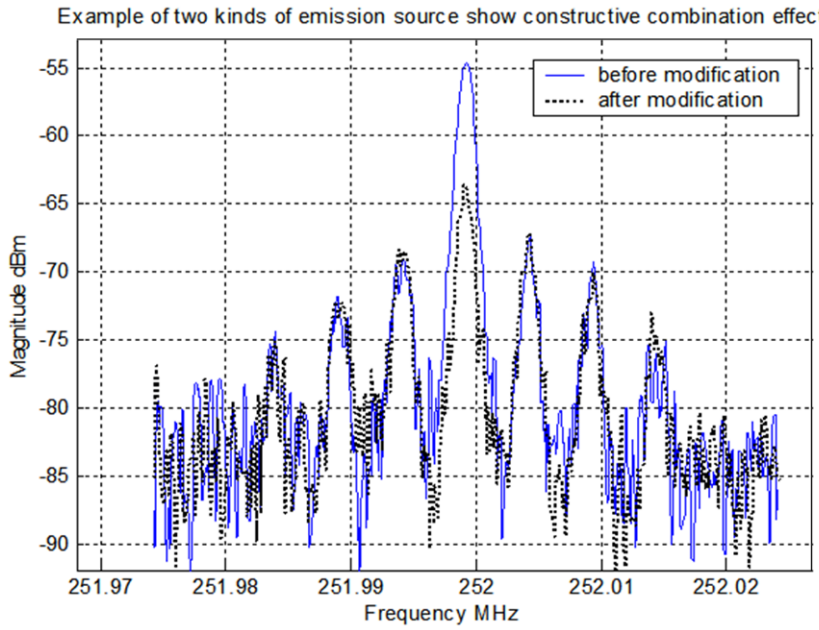

Figure 1.6. Far-field before and after a modification at 252 MHz. Only the signal having no sidebands is reduced by the modification.

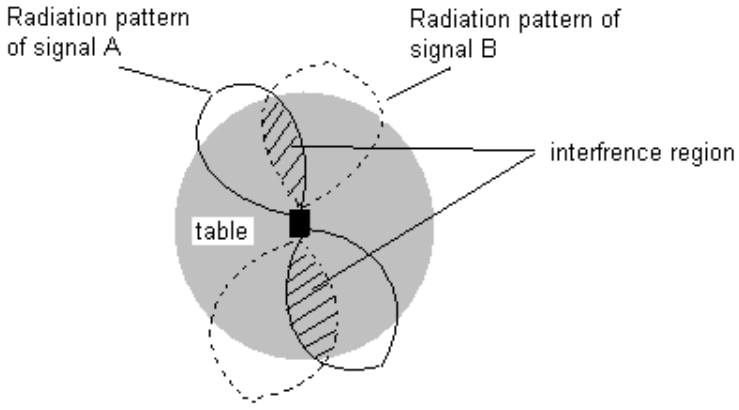

Figure 1.7. Two sources distinguished by the sidebands pattern have different antenna structures, thus different radiation patterns.

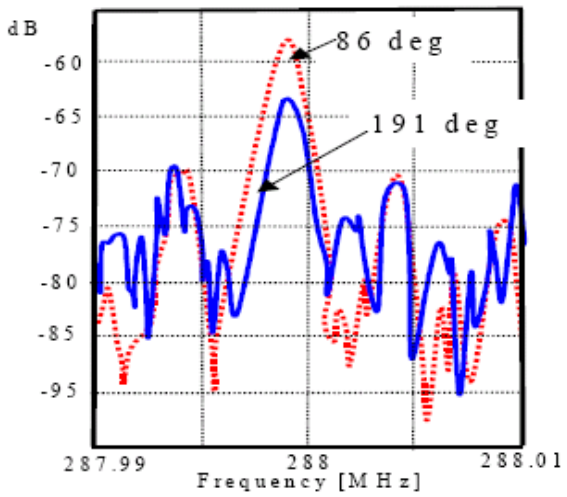

Figure 1.8. Far-field spectrum around 288 MHz for two turn-table positions.

1.4. ZERO SPAN MEASUREMENT

Two signals may have similar sideband magnitudes, but different modulations. Amplitude modulation (AM) cannot be distinguished directly from small-angle frequency modulation (FM). IQ demodulation or a time domain view helps. IQ demodulation is not implemented in many spectrum analyzers, but zero span can reveal the amplitude demodulated signal, provided that the modulation frequency is less than half of the largest RBW of the spectrum analyzer.

The center frequency of the spectrum analyzer is set to the frequency of interest using 0 Hz span, so that the horizontal axis shows time instead of frequency. The RBW must be larger than the spectrum occupied by the modulation, and the sweep time needs to be adjusted to see the AM modulation.

Typically, switched power supplies have switching frequencies between 30 kHz and 3 MHz. Data stream AM modulation can have a much broader range, whereas periodic jitter of PLLs has no amplitude modulation.

Zero span measurement reveals how the amplitude changes with time for any modulated RF signal within a specified bandwidth. Zero span measurement is quite useful to understand which switched power supply is causing a broadband noise. The example in Figure 1.9 shows the zero span measurement result on the 270 MHz signal captured in broadband measurement data shown in Figure 1.2. The amplitude of this resonance is apparently modulated by a signal with 120 Hz (T = 8.2 ms) fundamental frequency.

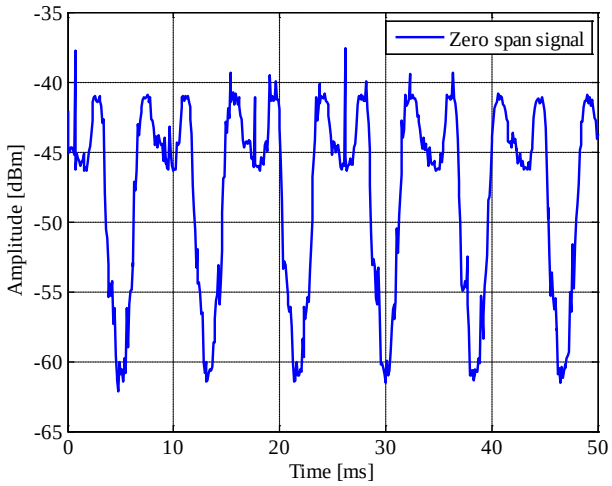

Figure 1.9. Zero span measurement (RBW = 10 MHz) of the signal in Figure 1.2 at 270 MHz.

1.5. CONCLUSION

This is the first article of a series covering different techniques for EMI failure analysis. It presented an overview of the EMI analysis techniques, and started with the basic measurements that can be done with a spectrum analyzer to obtain more information relative to the standard settings. The next article will cover time domain methods and the time varying spectral content of signals.

REFERENCES

[1] http://www.fcc.gov/oet/info/rules, FCC Rules & Regulations, May. 2009.

[2] David A. Weston, Electromagnetic Compatibility: Principles and Applications. Marcel Dekker Inc, 2001.

[3] Werner Schaefer, "EMC Narrowband and Broadband Discrimination with a Spectrum Analyzer or EMI Receiver," Conformity, Dec, 2007.

2. EMI FAILURE ANALYSIS: II. JOINT TIME-FREQUENCY ANALYSIS

Weifeng Pan and David Pommerenke, with contributions from all members of the EMC Laboratory at Missouri University of Science & Technology

2.1. INTRODUCTION

Time domain and frequency domain are two extremes of a large set of signal analysis techniques. Time domain gives the best time resolution, but no direct frequency information. The best frequency resolution is obtained in the frequency domain where, however, time variations of the signal are not visible. Joint time-frequency analysis allows moving continuously between time and frequency domain; time resolution can be traded off for frequency resolution or vice versa. This approach reveals how the signal spectrum evolves over time. For instance, when a specific power MOSFET is turned on, the RF signal caused by this specific switching event can be identified. Other joint time-frequency analysis techniques exist [1]. This article focuses on the short-term Fast Fourier Transform (STFFT) for its easy implementation and fast calculation [2][3]**.** Using wavelet transformation will achieve better time/frequency resolution, but wavelet computation is slower. Using STFFT, 2 mega samples of time domain data can be analyzed in seconds over the complete frequency range. As a second step, wavelet analysis can be used to focus on specific switching events [4]. Good examples of this approach are available at [5].

The principle method of the STFFT can be illustrated as: a long time-domain data set is cut into many small segments. The discrete-time Fourier Transform (DFT) of each segment is computed to generate its short-term frequency content. The time resolution

and frequency resolution can be adjusted by changing the data length of each segment. A better time resolution requires shorter time length of each segment, whereas a better frequency resolution needs more data in each segment. Other parameters, such as segment overlap and window function, influence the resolution. The basic process of STFFT is illustrated in Figure 2.1.

The STFFT method is often used to identify the source of emissions in complex systems where multiple broadband sources exist, such as switched power supplies with DC-DC converters. The identification is made by comparing the STFFT result of each local source with that of the far-field signal.

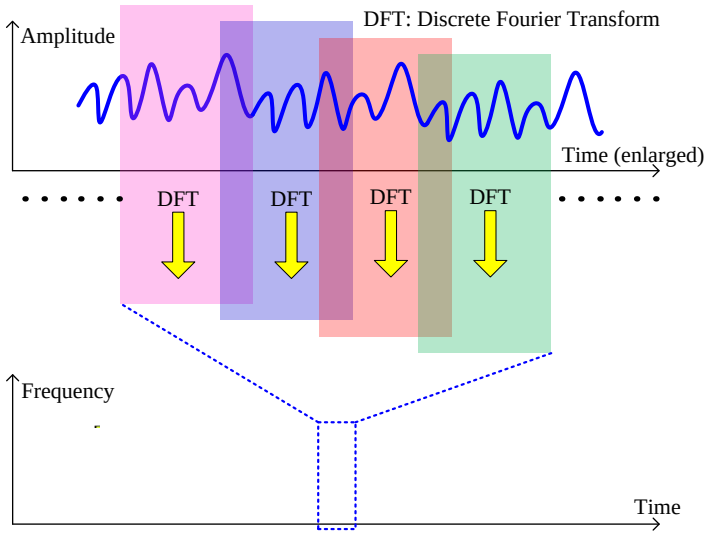

Figure 2.1. Basic STFFT process.

The signal is measured in time domain by an oscilloscope. Other instruments, such as a real-time spectrum analyzer from Tektronix or equivalent instruments from Agilent or National Instruments, can provide a similar analysis; however, they are usually

limited to a sampling bandwidth of 200 MHz or less. A broadband oscilloscope, on the other hand, is usually available, and it offers GHz bandwidth. We often use 2 mega samples at 5 GSa/sec, which gives a 400 μs capture window. A low pass filter, with a stop frequency of 1 GHz or so, is also needed at the input to avoid aliasing. If much slower processes need to be captured, such as a video signal with a repeat rate of 16.6 ms, the recording and processing of sufficiently long data become difficult with the limited memory depth of the oscilloscope. In such cases, down-sampling or down-mixing techniques are useful; the basic idea is to move the spectrum of interest to a lower frequency, so that a lower sampling rate can be used.

2.2. APPLICATIONS OF STFFT

The insight provided by this transformation is illustrated below with three examples. Figure 2.2 shows the far-field signal at around 931 MHz from a desktop PC. The signal spreads over a bandwidth of 6 MHz; and its nature remains unclear until the STFFT is applied. Figure 2.3 shows a dithered clock, i.e., a clock frequency modulated by a sine wave.

The second example shows three views (Figure 2.4) of the far-field caused by a switched power supply. The spectrum analyzer reveals only a broadband signal at around 95 MHz; it does not reveal which switching edge is causing the emission, nor does it permit a distinction between various power supplies if all emit in the same frequency range. The time domain signal, however, reveals two switching events, i.e., the turning on and off of a MOSFET. The switching rate is about 0.6 μs. In the STFFT we see the

spectral energy of both switching events, one covering a broader bandwidth and the other with its energy concentrated around 95 MHz.

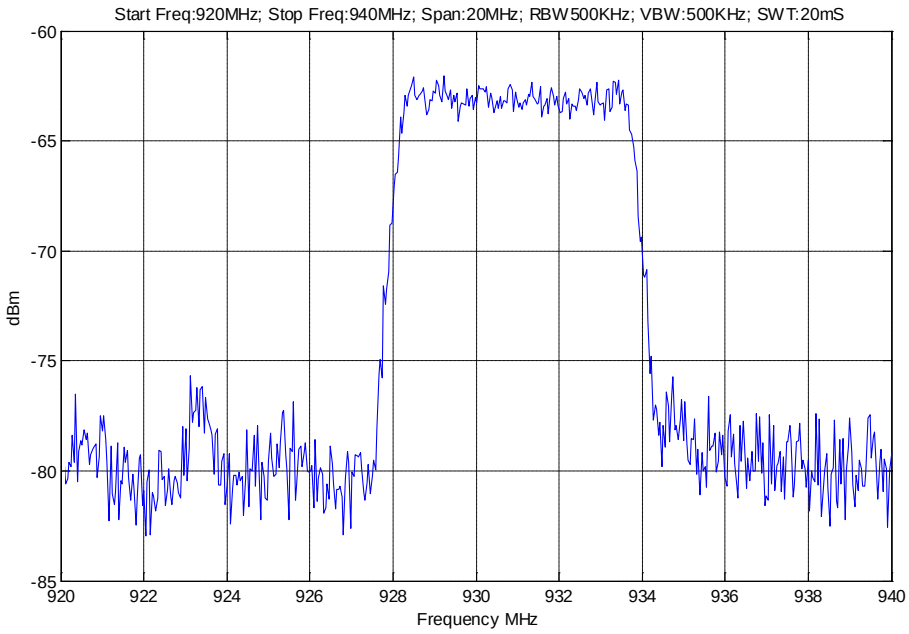

Figure 2.2. Narrowband spectrum at 931 MHz of a far-field signal.

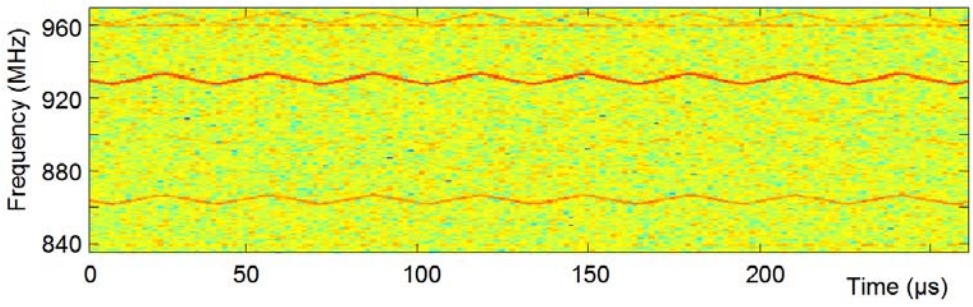

Figure 2.3. STFFT result zoomed in to 840 ~ 960 MHz, showing the dithered clock. Other dithered signals are visible at 860 MHz and 960 MHz.

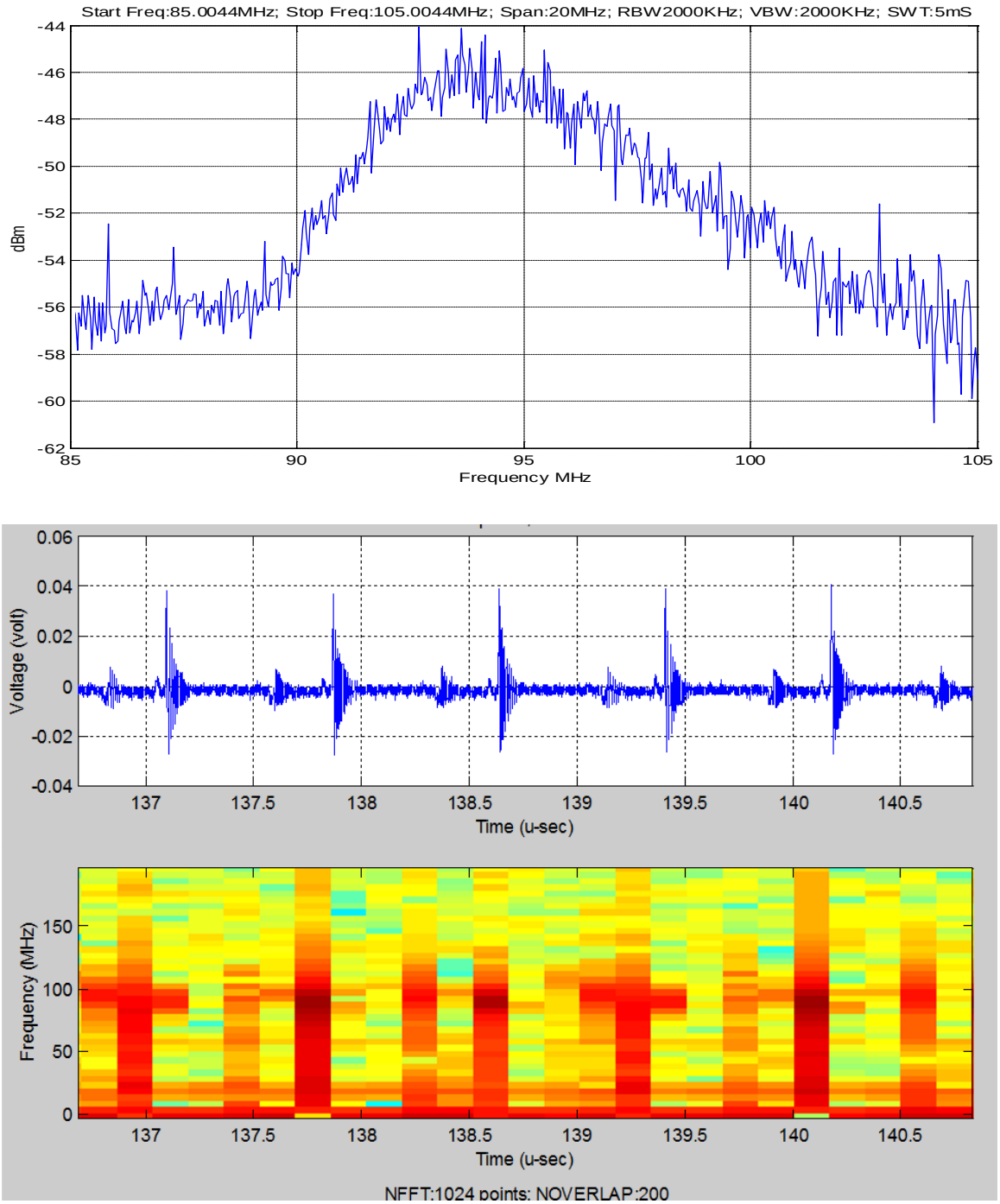

Figure 2.4. EMI of a switched power supply. Top: spectrum analyzer peak detection of the far-field signal. Middle: time domain waveform. Bottom: STFFT of the time domain signal.

One further example of a switched power supply causing EMI problem is shown in Figure 2.5. Strong 280 MHz centered broadband emissions were observed in the STFFT. The circuit was a synchronous DC-DC buck converter, with a typical circuit topology [6] shown in Figure 2.6. The associated voltage in the buck converter, Vsw, is displayed at the bottom. The moment ($t \approx 1.732 \times 10^{-4}$s) of the strong broadband noise was aligned to a false switching event. The broadband pulse was caused by a control error in design, which allowed both FETs to turn on simultaneously. This error led to a very large current as the input 12V was shorted to reference by a few nano-Henries of inductance.

For complex broadband signals, such as data bus problems or systems having many switched power supplies, the STFFT technique is especially useful to identify the sources of emissions and to correlate individual switching events to far-field emissions. For narrowband signals, however, a spectrum analyzer is superior; it can provide kHz, even Hz resolution of signals close to the carrier. An FFT would require a very long data record. For example, if we capture 400 μs of data, the basic FFT resolution would be 2.5 kHz at best.

2.3. SUMMARY

During EMI failure analysis, a variety of techniques can be used for source identification. Table 2.1 explains a suggested measurement sequence for source identification in complex systems.

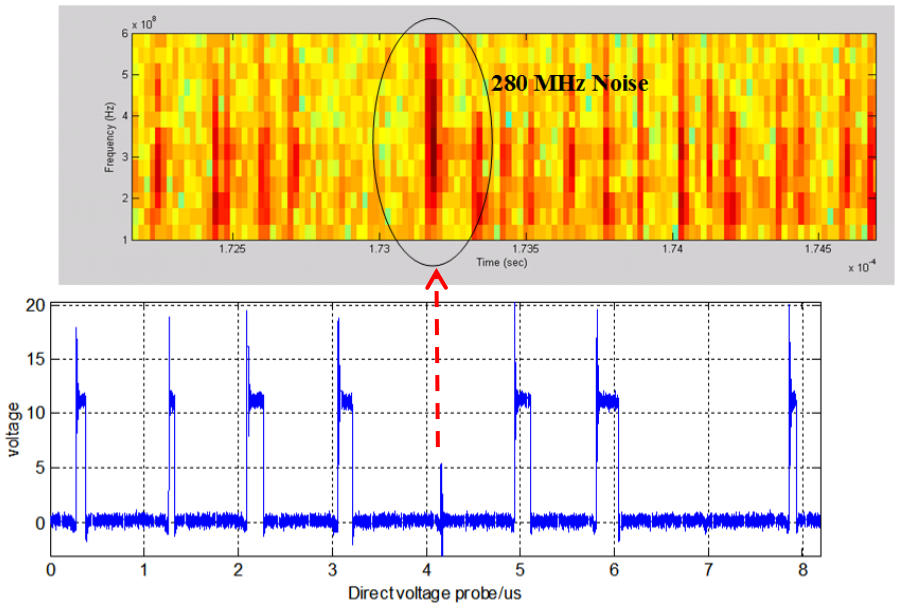

Figure 2.5. Strong 280 MHz centered broadband emissions shown in the STFFT domain (top) and associated voltage (bottom) in the buck converter. The broadband pulse was caused by a control error, allowing both FETs to turn on and leading to a very large current as the input 12V was shorted by a few nH of inductance.

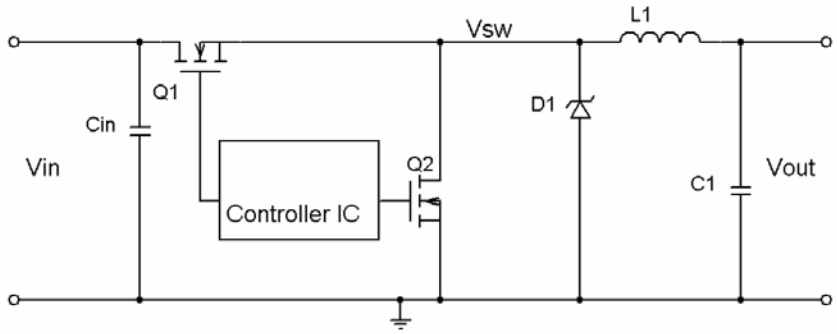

Figure 2.6. Typical circuit diagram of a synchronous DC-DC buck converter.

Table 2.1. Suggested measurement sequence for EMI source identification.

Measurement			Objective
1	Far-field measurement (frequency domain, peak hold)		Obtain an overview. Distinguish between narrow band and broad band signals.
1.1	Narrowband signals	Check for sidebands using kHz span	Identify possible modulations that will help to correlate far-field to many possible near-field sources.
		Zero span to check on signals having sidebands	Determine if sidebands are from AM or FM modulation.
1.2	Broadband signals: zero span		Determine switching frequencies.
2	Time domain measurement using oscilloscope attached to the far-field antenna		In depth analysis of broadband signals and modulation of narrowband signals.
2.1	Apply STFFT to time domain data.		Reveal how spectra change with time, e.g., identifying switching events in switched power supplies.
2.2	Attach near-field probe to second channel, and probe the EUT while observing the far-field in time domain.		Observe the timing between the far-field and the near-field to identify which switching event is causing the far-field signals.

Table 2.1. Suggested measurement sequence for EMI source identification (cont.)

2.3	Correlation analysis with synchronized measurement (to be covered in the following article in this series).	When multiple near-field sources potentially cause the emission at the same frequency and the near-field spectra cannot be visually correlated to far-field sideband signature, a mathematical correlation analysis can be performed.

2.4. CONCLUSION

This article, the second in a series of articles on EMI failure analysis, presented the joint time-frequency analysis techniques. STFFT analysis was introduced as a very useful method among a variety of source identification techniques. It intuitively displays the spectrum evolvement over time, offering a new perspective that cannot be achieved by separate time or frequency domain analysis.

REFERENCES

[1] S. Qian and D. Chen, “Joint time-frequency analysis,” Signal Processing Magazine, IEEE, Volume 16, Issue 2, March 1999.

[2] Kuisma, M. and Silventoinen, P., “Using spectrograms in EMI-analysis - an overview,” IEEE Applied Power Electronics Conference and Exposition, 2005. vol.3.

[3] Zhe Li and Pommerenke, D., “EMI-debugging of complex systems using different time, modulation, STFFT and frequency domain signal analysis techniques,” IEEE International Symposium on Electromagnetic Compatibility, 2005. vol.2.

[4] Wei Wu, “Continuous wavelet transform application in electromagnetic compatibility - algorithms and software realization,” SoftCOM 2007.

[5] http://www.emcexplorer.com, EMCExplorer, May 2009.

[6] Abraham I. Pressman, “Switching Power Supply Design,” 2nd Edition, McGraw-Hill, 1998, pp. 413 – 426.

3. EMI FAILURE ANALYSIS TECHNIQUES: III. CORRELATION ANALYSIS

Weifeng Pan, Gang Feng, and David Pommerenke

EMC Laboratory, Missouri University of Science & Technology

3.1. INTRODUCTION

Locating the emission source can be the most challenging part in EMI failure analysis. In the previous article [1], a measurement sequence for source identification in complex systems was suggested. A variety of methods can be used to find the correlation between the far-field and a near-field signal. The correlation can be a similarity either in frequency spectrum or in time domain, or in joint time-frequency signatures. When multiple near-field sources potentially cause the emission at the same frequency and the near-field spectra cannot be visually correlated to far-field sideband signature, a mathematical correlation analysis can be performed [2]. Some commercial systems are also available [3][4].

3.2. MATHEMATICAL CORRELATION METHODS

The EUT used in this article to illustrate the methodology had broadband emission centered at 667 MHz. This radiated emission frequency is created by many ICs and modules as one harmonic of the clock and data signals. Several suspected EMI sources and their coupling paths were located, e.g., ICs with a heat sink, high speed signal cable bundles and a USB connector.

The correlation analysis requires time-synchronized measurement of the far-field and near-field signal. This can usually be implemented by using two channels on an oscilloscope, as shown in Figure 3.1. The use of band pass filters is advised to attenuate signals that are not of interest and to achieve a better signal to noise ratio.

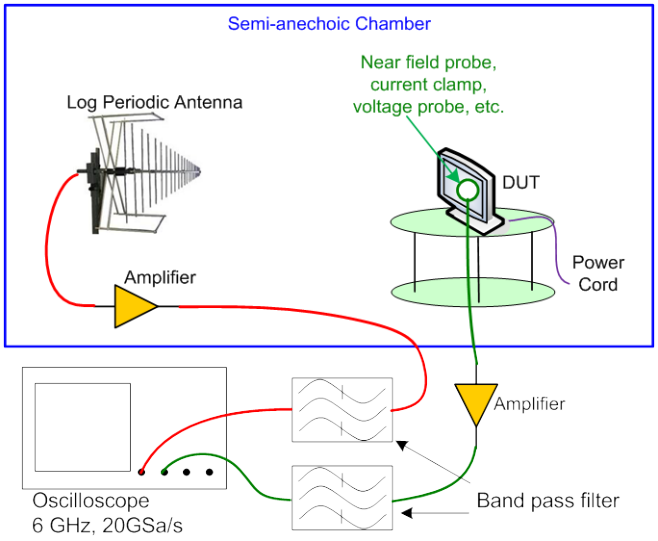

Figure 3.1. Time-synchronized measurement of far-field and near-field for correlation analysis.

Depending on the local quantity, a variety of test accessories can be used. We typically use E-field or H-field probes, current clamps or direct voltage measurements (to capture signals or voltages between “grounds” or metal parts).

There are several correlation analysis methods listed in Table 3.1. These methods have been in practical use in our EMC lab. Some of them will be covered in this article.

Table 3.1. Overview of the correlation methods.

Correlation Method	Brief description
STFFT	Correlate the time changes of the spectral composition.
Direct correlation	Determine the correlation coefficient between the time vectors.
Envelope correlation	Determine the signal's envelope first and then analyze the correlation between the time changing envelopes.
Amplitude density distribution	Analyze the amplitude density distribution of two signals to compare between near-field and far-field.
Sideband analysis	Compare phase noise or sideband of signals in the near-field to the far-field signal.
Timing analysis	Compare the timing of events in the near-field to timing observed in the far-field signal.

3.2.1. STFFT Correlation. As introduced in the second article [1], the STFFT displays the spectral content of a signal in time domain. The correlation between the STFFT spectrograms of the near-field and far-field signal is a good indication of the likeliness of a near-field signal to be the EMI source. The STFFT result of a near-field signal and the far-field is shown in Figure 3.2. The near-field signal was the output from a current clamp around the high speed signal cable. The first and second plot show that the near-field signal is amplitude modulated by pulses of different width. Its spectrum is symmetrical. The far-field signal in the third and fourth plots is very noisy. It is a combination of three signals: an amplitude modulated signal similar to the near-field

signal, a clock signal at 663.5 MHz, and a noise-resembling signal with a wide spread and even spectrum. There is a noticeable dropout of the near-field signal in the time waveform from 4300~5000 μs. However, the corresponding dropout can barely be seen in the far-field signal, because this dropout is overwhelmed by other signals. The STFFT analysis indicates the measured near-field signal counts only a small fraction of the total radiated emission centered at 667 MHz. The correlation between this near-field signal and the far-field signal is weak. Other analysis techniques will be used to identify the correlation to this complicated far-field signal.

3.2.2. Envelope Correlation. As it's already seen, amplitude modulated signals are very common in EMI analysis. The envelope of the time domain amplitude is an important attribute of the amplitude modulated signals. Here the definition of envelope is on a specified carrier frequency. It's the spectrum amplitude at that frequency versus time. After capturing the time domain data, their envelopes need to be determined. One way to do so is to extract the envelope from the amplitude data of the STFFT spectrogram at the carrier frequency, i.e., to plot one row of data in the STFFT spectrogram. This can also be achieved by using zero span measurement on a spectrum analyzer. However, if the envelope is changing randomly, time-synchronized measurement of two channels is necessary, which cannot be done on most spectrum analyzers.

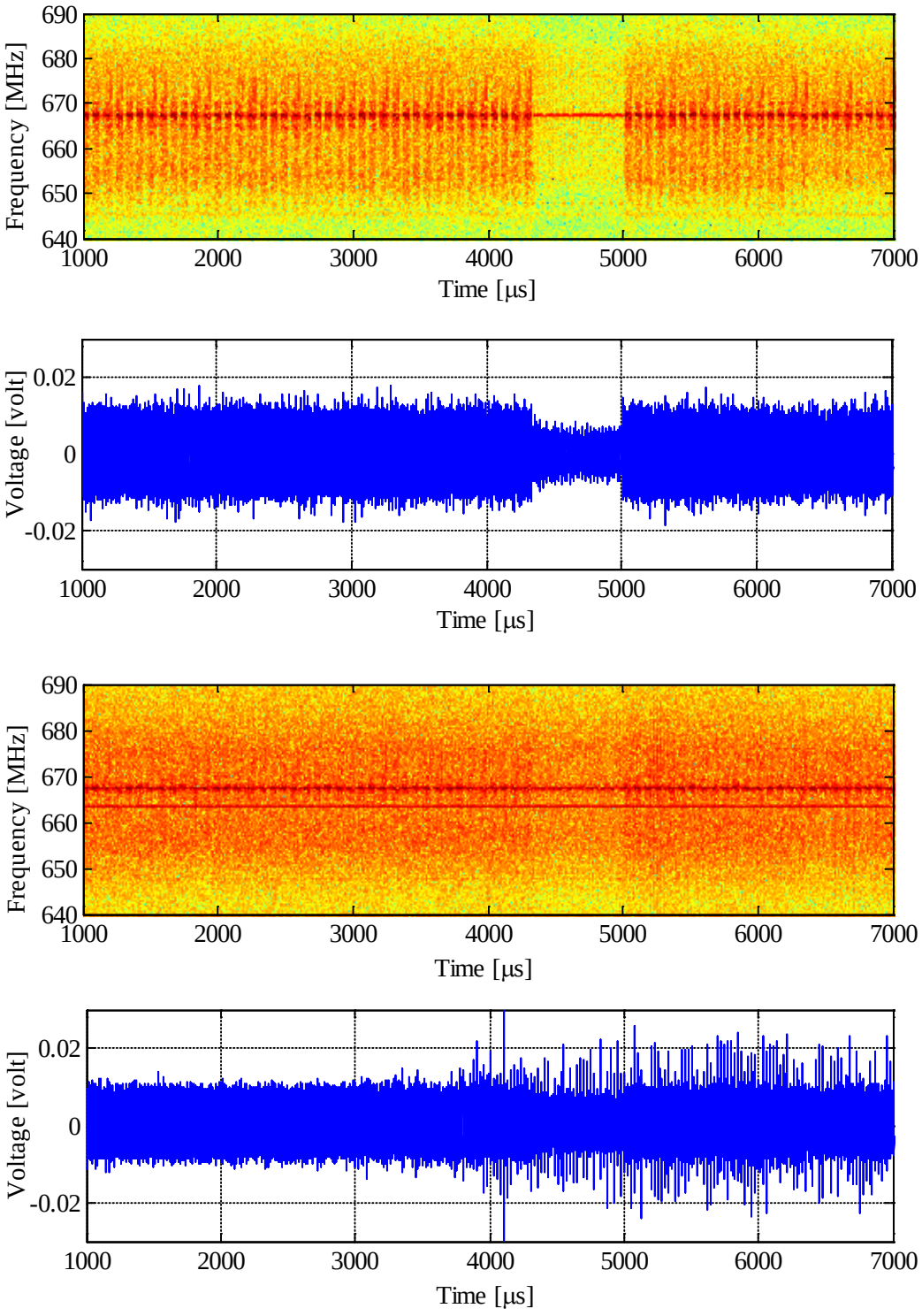

Figure 3.2. STFFT spectrograms (1st and 3rd plots) and time domain waveforms (2nd and 4th plots) of near-field and far-field signals.

Cross-correlation function can be used to compare the envelopes of two signals. The cross-correlation of two discrete signal sequences is defined as:

$$R_{xy}(m) = E\left\{x_{n+m}y_n^*\right\} = E\left\{x_n y_{n-m}^*\right\} \tag{3.1}$$

where x and y are jointly stationary random processes and $E\{\}$ is the expected value operator. R_{xy} will be zero when x and y are uncorrelated. If the two processes are correlated, R_{xy} will reach its maximum value when m is equal to the time lag between the two processes. In practice, only a finite segment of the infinite long random process is available. The cross-correlation of two discrete signal segments [5], x and y, each with a length of N is defined as:

$$\hat{R}_{xy}(m) = \begin{cases} \sum_{n=0}^{N-m-1} x_{n+m}y_n^* & m \geq 0 \\ \hat{R}_{xy}^*(-m) & m < 0 \end{cases} \tag{3.2}$$

Extract the envelopes at 667 MHz from the far-field and a near-field signal, as shown in Figure 3.3. They are both amplitude modulated by periodical signals. The correlation function in the bottom plot indicates that the two envelopes have the same periodicity of about 15 μs. This confirms that this near-field signal and the far-field signal are amplitude modulated by one same signal.

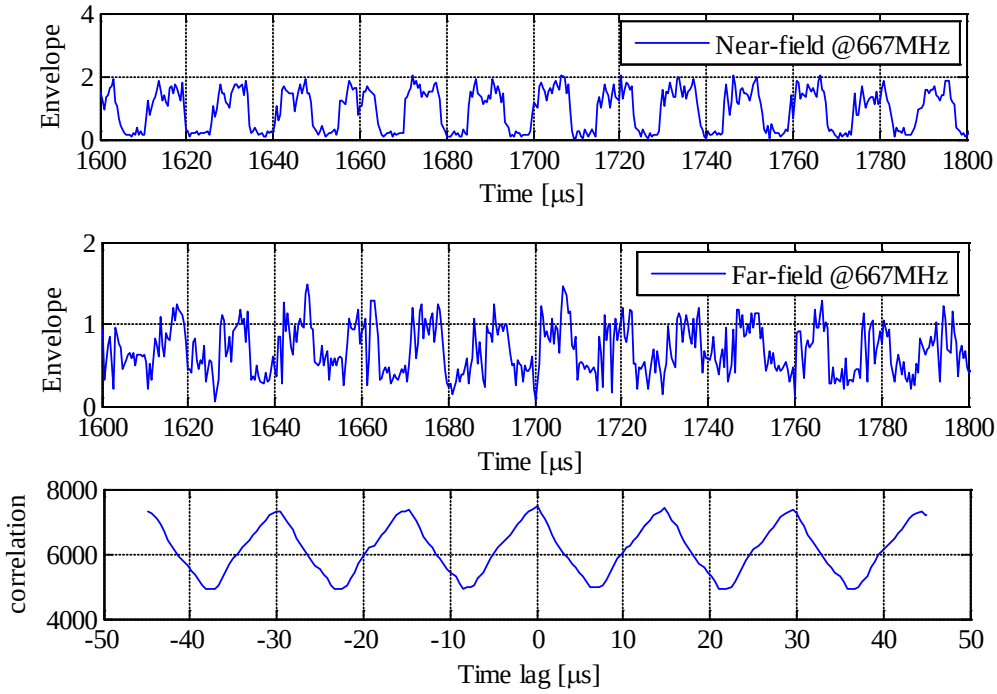

Figure 3.3. Envelope at 667 MHz of a near-field signal (top) and the far-field (middle). Bottom: the cross-correlation of these two signals.

3.2.3. Coherence Factor. A more direct way to find the relation between two signals is to calculate the coherence factor for their frequency spectra. The coherence factor is defined as:

$$C_{xy}(f) = \frac{\left|P_{xy}(f)\right|}{\sqrt{P_{xx}(f)P_{yy}(f)}} \tag{3.3}$$

where P_{xy} is the cross power spectral density of sequences x and y; P_{xx} and P_{yy} are the power spectral density of sequence x and y respectively. Coherence factor is a function of frequency, with a value between 0 and 1. If two signals are linearly related, the

coherence factor will be “1” for all frequencies. A coherence factor of “0” indicates that two signals are not related at that frequency.

The results of coherence factor analysis are shown in Figure 3.4. The Y axis is in log scale. Because band-pass filters centered at 667 MHz were used in these measurements, the peaks outside the pass-band are a result of random noise. A fairly strong coherence can be observed in the narrow frequency band around 667 MHz. When near-field data measured at different locations of suspected EMI sources are available, the coherence factor can be used to determine which near-field signal best correlates to the far-field signal.

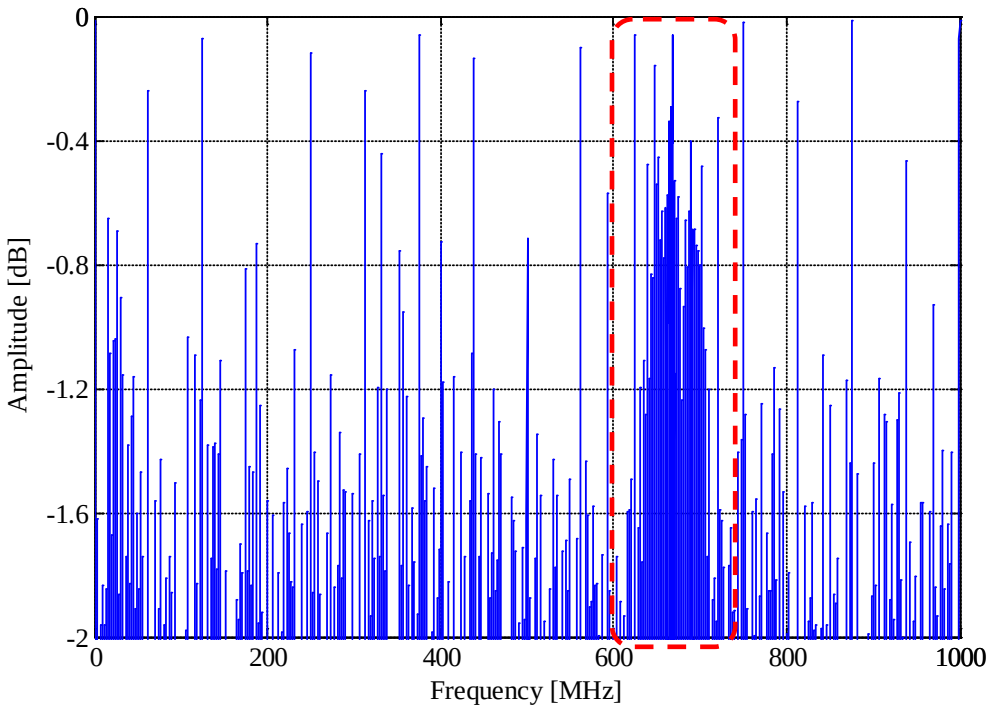

Figure 3.4. Coherence factor between a near-field signal and the far-field signal.

3.2.4. Direct Correlation. Direct correlation is to do a cross-correlation calculation between two-time synchronized waveforms. Figure 3.5 shows the direct correlation between a near-field signal and the far-field. The maximum peak is at -35.5 ns, which suggests the far-field has 35.5 ns time lag to this near-field. The delay is caused by different signal paths of the near and far-field measurements, which include distance to antenna, cables, and devices such as filters and amplifiers. In the case where several near-field signals are found to be correlated to the far-field, the signal which is the earliest in time has the best chance to be the EMI source.

The separation between the peaks in the bottom plot of Figure 3.5 is about 15 ns, corresponding to the main signal at 667 MHz in both near and far-field. The envelope of the cross-correlation also has a repetition of 0.367 μs, corresponding to the 2.7 MHz amplitude modulating signal in both near and far-field. In summary, the direct cross-correlation of two time domain waveforms effectively reveals the delay and periodicity information of two correlated signals.

3.2.5. Amplitude Density Distribution. The amplitude density distribution shows the probability for the amplitude of a time domain waveform to occur at a certain value. In general, two well correlated signals should have the similar amplitude density distribution. Exceptions to this can occur in non-linear systems, where the input and output signals can have similar spectral information, but totally different amplitude distributions. Further, one cannot remind often enough that correlation is not a measure for causality. Two similar amplitude distributions do not necessarily mean two signals are well correlated. It requires further information to show causality. In our experience the amplitude density distribution turned out to be useful for excluding causality.

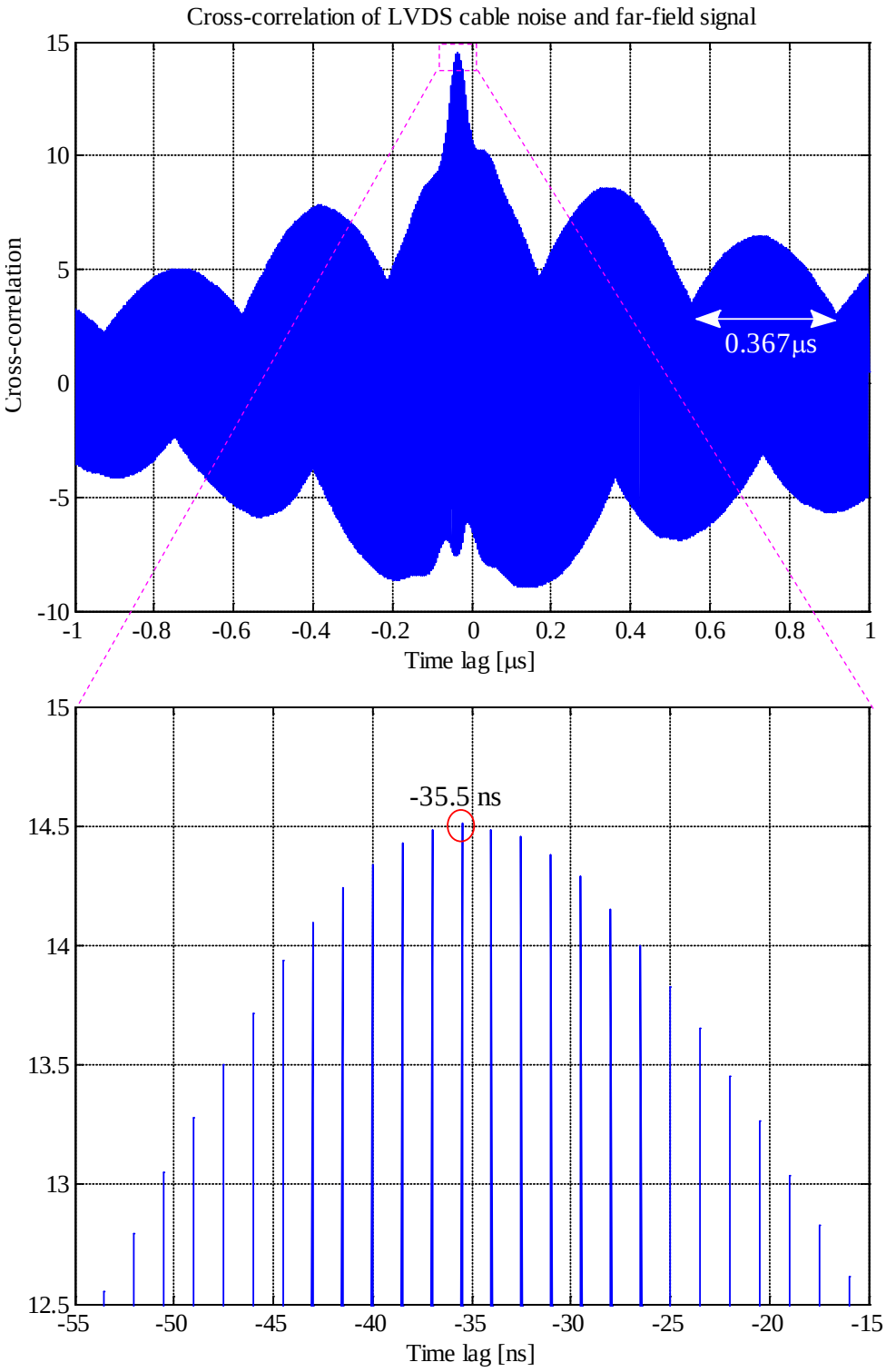

Figure 3.5. Direct correlation of a near-field signal and the far-field.

The amplitude distribution comparison between the far-field signal and a near-field signal in Figure 3.6 shows pretty good similarity. Both are somewhat Gaussian-shaped. Of course, it should be ensured that the time domain data has sufficiently good signal to noise ratio. Otherwise the amplitude density distribution of the noise, which is also Gaussian-shaped, would dominate.

In another case, presented in Figure 3.7, the amplitude density distribution of a near-field signal is very different to that of the far-field signal. This indicates that the emission from this source contributes very little, if any, to the far-field.

3.3. CONCLUSION

This paper introduced five essential correlation analysis techniques for identifying EMI source and coupling path. Correlation analysis helps determine the inter-relation between multiple near-field signals and the far-field signal. When applicable, multiple correlation techniques should be used to reveal more information on the correlation between the signals. Correlation analysis is also an important step in the recommended measurement sequence [1] for EMI source identification. It is an advanced measurement and data analysis method, which requires complex hardware for multi-channel time-synchronized measurement and extensive post-processing of measured data.

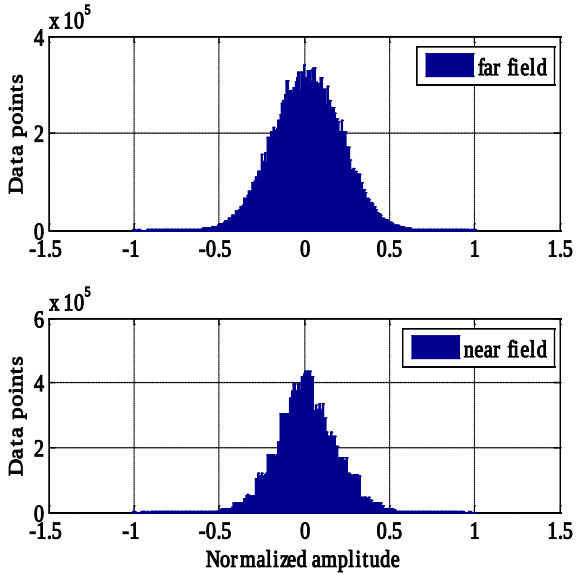

Figure 3.6. Comparing the amplitude density distribution of far-field and a near-field signal. Both have Gaussian-shaped distributions.

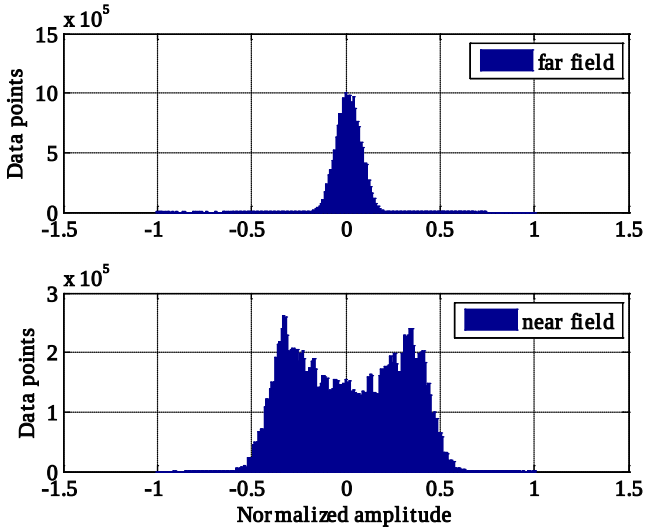

Figure 3.7. Amplitude density distribution of the far-field and from a signal captured by current clamp.

REFERENCES

[1] Weifeng Pan and Pommerenke, D., “EMI Failure Analysis Techniques: II. Joint Time-Frequency Analysis.”

[2] Gang Feng, Wei Wu, Pommerenke, D., Jun Fan, Beetner, D.G., “Time synchronized near-field and far-field for EMI source identification,” IEEE International Symposium on Electromagnetic Compatibility, 2008.

[3] http://www.sara.com/EM/cassper/index.html, CASSPER system, SARA, Inc. May 2009

[4] Parhami, P., Marino, M., Watkins, S., Nakauchi, E., “Innovative pre-compliance test methodology using ambient cancellation and coherence detection techniques,” IEEE International Symposium on Electromagnetic Compatibility, 1999, vol.2.

[5] Orfanidis, S.J., “Optimum Signal Processing. An Introduction,” 2nd Edition, Prentice-Hall, Englewood Cliffs, NJ, 1996.

4. PREDICTING NOISE VOLTAGE FROM TRACE CROSSING SPLIT PLANES ON PRINTED CIRCUIT BOARDS

Weifeng Pan[1], David Pommerenke[1], Samuel Connor[2], Bruce Archambeault[2]

[1]EMC Lab, Missouri University of Science & Technology, Rolla, MO 65401

[2]IBM Corporation, 3039 Cornwallis Rd, Research Triangle Park, NC 27709

4.1. ABSTRACT

Printed circuit Boards (PCBs) often have high speed data traces crossing splits in the adjacent reference planes due to space limitations and cost constraints. These split planes are usually different power islands on nearby layers. This work develops an equivalent inductance to quantify the effect of the split plane and the associated stitching capacitor for various stack-up configurations.

Researching the effect of a trace crossing a gap can be motivated by different questions and applications. From an SI point of view, one may ask for the effect of the slot on the trace current. While RFI, EMI, and to some extend cross talk problems are more interested in the voltage across the slot, even if it is so small that its effect on the trace current can be neglected. The outcome of the analysis may then take different paths. The user may want to obtain:

- Physical insight by approximating the effects within a complex structure by a small number of highly simple structures. Modeling the slot as a slot line is an example.
- Analytical description.
- Usable design curves, parameters or empirical equations. The understanding of the physics is here only needed for validating the results, but the results can

be expressed in a form that totally hides the physics. The result quantifies relevant parameters of the problem.

This approach is similar to the previous with the difference that only bounds are determined. Thus, much stronger worst case assumptions can be used. The work presented quantifies the effect of the slot in form of an inductance which is derived using worst case voltages.

4.2. INTRODUCTION

Splits in the power or ground planes are typically used to introduce DC isolation between different supply voltages [1], to isolate RF signals from digital signals, or to isolate low noise analog from digital circuits. Under special I/O circumstances, intentional splits are used to minimize radiated emissions [2]. It is well known that high speed traces should never be routed across a reference plane split in an adjacent layer. However, due to the demand for smaller board size and less number of layers, there is often little flexibility to use optimum trace routing. In many circumstances high speed signal traces have to run across splits between reference planes, even though EMC and signal integrity design rules would advise against this design practice.

It is also well known that the high frequency harmonic content of the data signal's current takes the nearest reference plane as its predominant return path. If a split in this reference plane exists, it will cut off the path for the conduction current and induce noise voltage across the split. The impact of trace crossing split planes on both signal integrity and EMI has been analyzed and evaluated in [3]-[6]. One counter-measure is to use stitching capacitors across the split to reduce impedance in the current return path. The

effect of stitching capacitor distance for critical traces crossing split reference planes was discussed in [7].

The split planes being studied are often stand-alone planes. But for practical cases on a real PCB, the split planes are often part of certain power plane structures. Power planes and their decoupling capacitors may provide another significant current return path because of their low impedance. Figure 4.1 gives a depiction of the current flow for the case of a microstrip crossing a split. Part of the return current may flow along the split and take the path via the stitching capacitor. The rest of the current may go via the power plane structures. To predict the amount of voltage induced across the split, both paths need to be considered. The equivalent circuit model is shown in Figure 4.2, where I_{return} is the total return current on reference plane, $C_{stitching}$ is the capacitance of the stitching capacitor, *ESL* is the equivalent series inductance of the stitching capacitor, L_{via} is the via connection inductance of the stitching capacitor [8], $L_{equivalent}$ is the inductance from the discontinuity for the return current on the split plane, Z_{pp_left} and Z_{pp_right} are the power plane impedance looking from the slot to the left and right respectively, C_{slot} is the capacitance across the slot when the slot length is electrically small. C_{slot} is fairly small and can be neglected when power planes are present.

There are several approaches to compute the slot voltage. Full wave numerical modeling methods can be used to provide a good estimation of the amount of noise voltage induced across the split. However, these tools require careful use, and take a significant amount of time and are not practical for a quick engineering answer.

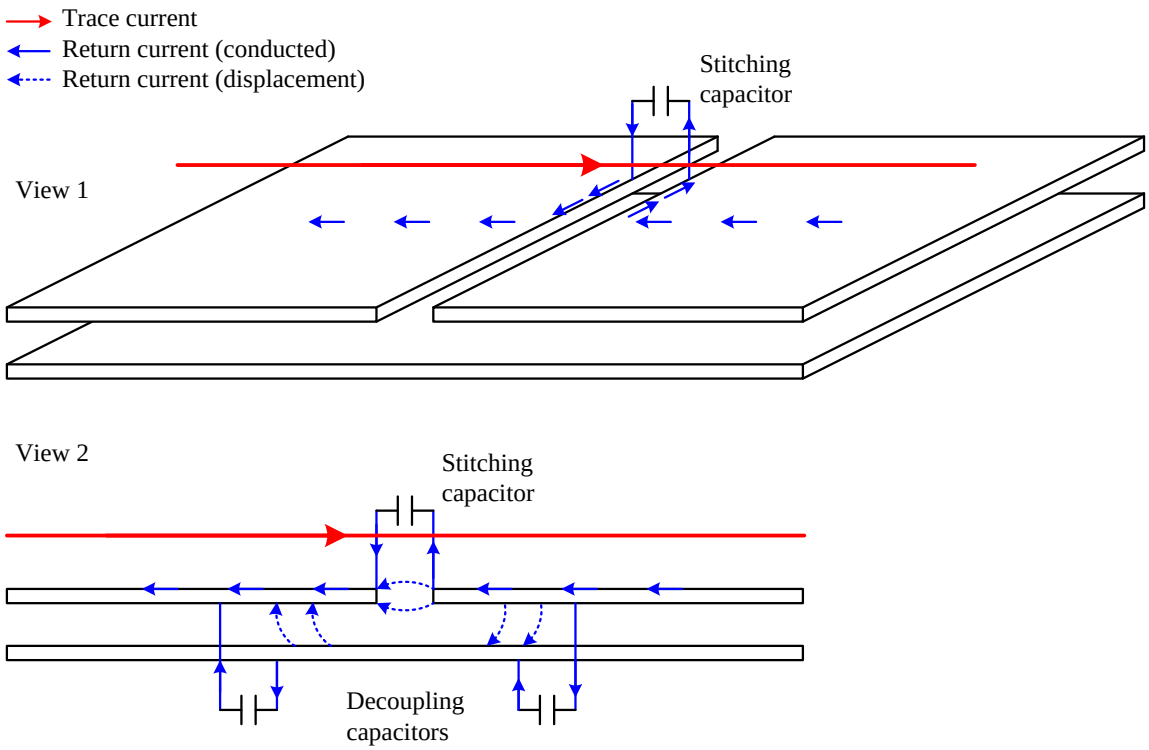

Figure 4.1. A depiction of the current flow for a microstrip crossing split planes.

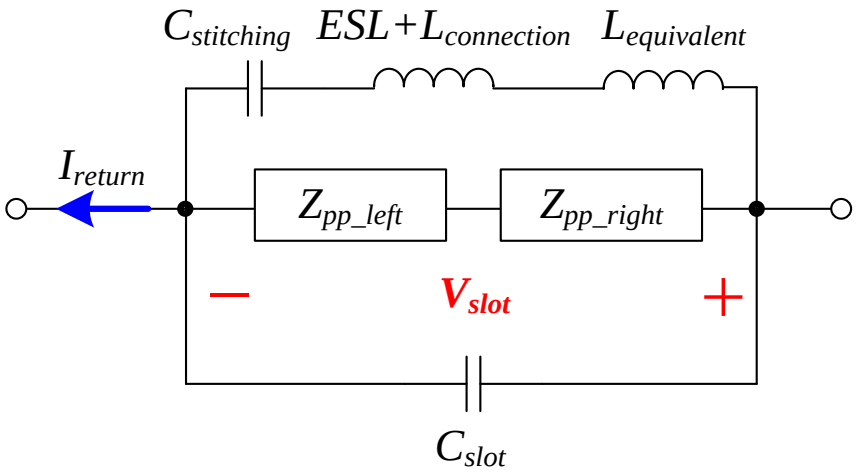

Figure 4.2. Equivalent circuit model of the case in Figure 4.1.

Modeling the slot as transmission lines is also an effective approach [3][9]. The case of microstrip with a single split plane is modeled with transmission lines in Figure 4.3, where C_x and L_x are from the signal trace section above the slot. But this approach has difficulty in handling structures where the signal trace is a stripline or where there is a solid plane adjacent to the split plane to form power planes.

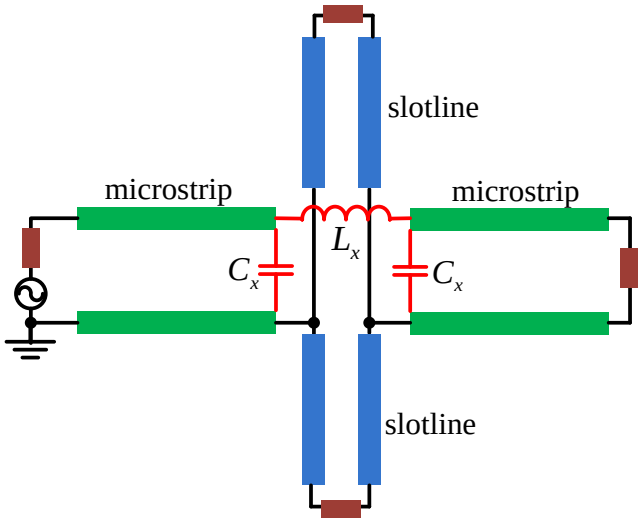

Figure 4.3. Transmission line model of microstrip crossing a slot.

The approach of effective ground inductance [10] is to model the overall impedance caused by the discontinuity of split as an inductor. This may work only when the split planes are not part of the power plane structures and when the frequency is not high enough for C_{slot} to be decisive. With these two prerequisites, the equivalent circuit model in Figure 4.2 is dominated by *ESL*, L_{via} and $L_{equivalent}$. Using a frequency-dependent effective ground inductance to calculate the voltage amplitude in frequency domain does not render any phase information. Thus, it makes time-domain simulation impossible.

Based on the equivalent circuit model in Figure 4.2, this paper discusses the development of $L_{equivalent}$ (L_e hereafter) for the calculation of the noise voltage across the split under common PCB layer configurations, including microstrip and stripline. The derivation of L_e takes into account the width of the split *s*, the distance of the stitching capacitor to the center of the signal trace *d*, and the separations between trace and planes *h*. Using this equivalent inductance together with other parameters in the equivalent circuit, the maximum voltage across the split can be calculated using the intentional signal current on the trace, I_{trace}.

The noise voltage across the split, normalized to trace current, was found using a full wave simulation which employs the Finite-Difference Time-Domain (FDTD) method. A variety of stack-up configurations were modeled using EZ-FDTD [11] simulation software. Each model has one signal trace and one shorting tab (as a perfect stitching capacitor) connecting the two split planes. While the signal may also be on many traces (bus) [6] or differential pairs [12], the effect of the noise across the split will be a superposition. Finally, some measurement validation of the simulation results for the microstrip configuration will be discussed.

4.3. MICROSTRIP CONFIGURATION

Split in the microstrip reference plane is the simplest and most often discussed structure among all the split plane cases. In the FDTD model shown in Figure 4.4, the cell size is 0.5 mm, 0.25 mm and 0.1 mm along X, Y and Z axis. The trace has 1 mm width and 0.3 mm height above the reference plane. Air dielectric is used within the structure, thus the characteristic impedance Z_0 is about 57 Ω. It has been verified that the

presence of dielectric or the value of Z_0 is almost irrelevant to the amount of voltage induced across the split. The source and load are matched to Z_0. The split is in the middle of the reference plane, with both ends terminated with resistors. The termination of the split is to avoid length dependant resonances, and to obtain a more general length independent result. The value of the slot termination resistance was verified by observing no reflection from the end of the slot. Voltage probes are placed along the slot.

The source voltage is a Gaussian pulse. As we assume that the slot does not significantly affect the trace current, the current on the trace $I_{\text{trace}}(t) = V_{\text{source}}(t)/2Z_0$. When the pulse is launched along the microstrip and hits the split, noise voltage on the probes along the slot are observed. An example of the voltage waveforms from FDTD simulation result is shown in Figure 4.5, where $d = 12$ mm and $s = 0.5$ mm.

I_{trace} and the voltage waveforms were transformed by Fast Fourier Transform (FFT). At each frequency point, the maximum voltage among all the probes was recorded then normalized to the FFT amplitude of I_{trace}. Thus, there is a transfer impedance curve that relates V_{slot} to I_{trace}. All together, there were 27 such curves from 27 simulations by the combination of s (0.5, 1, 1.5 mm) and d (1, 2, 3, ⋯, 8, 12 mm). The value selection of s and d covers the most common board design geometry dimensions.

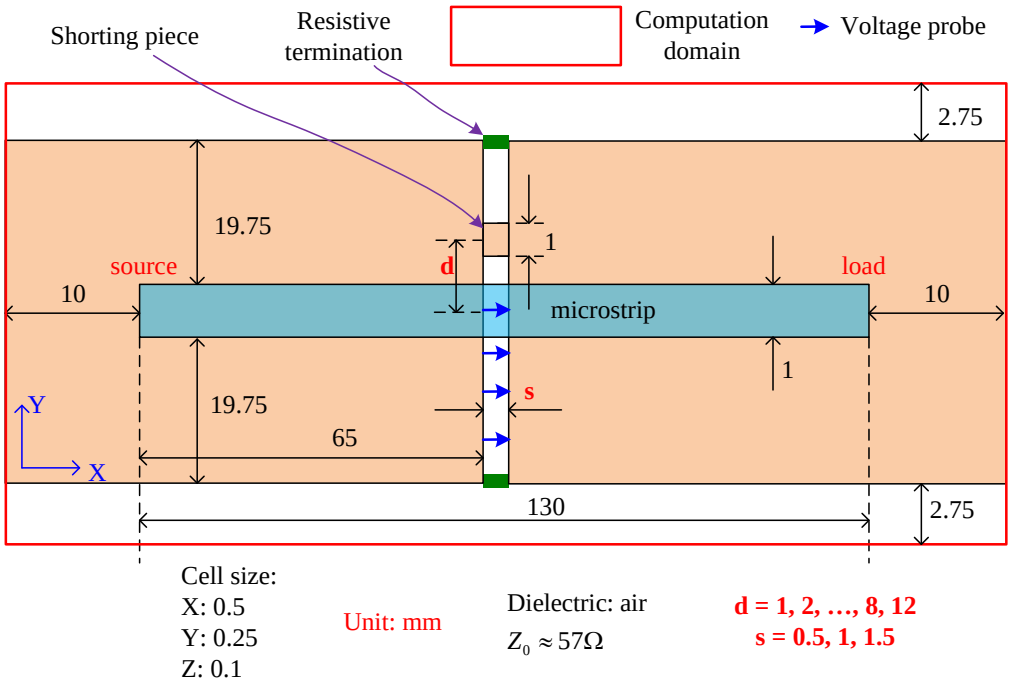

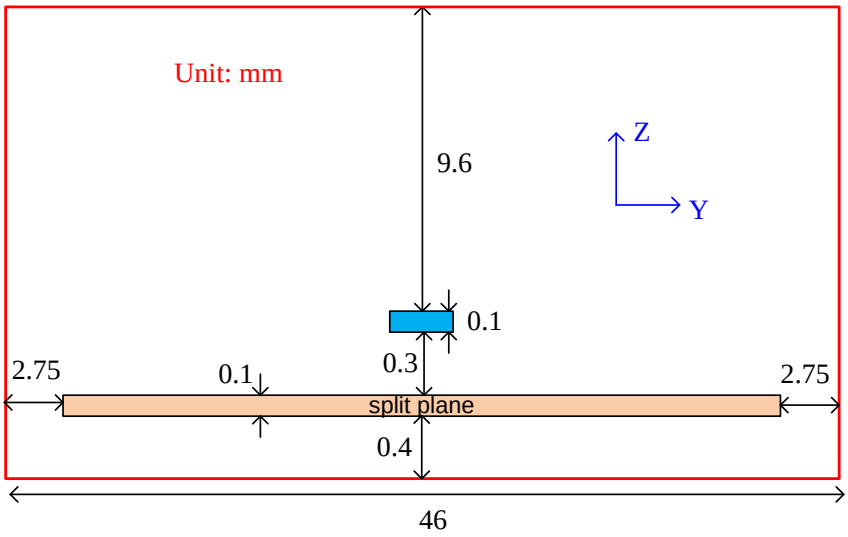

Figure 4.4. Simulation structure of a microstrip crossing split plane, top and cross section view.

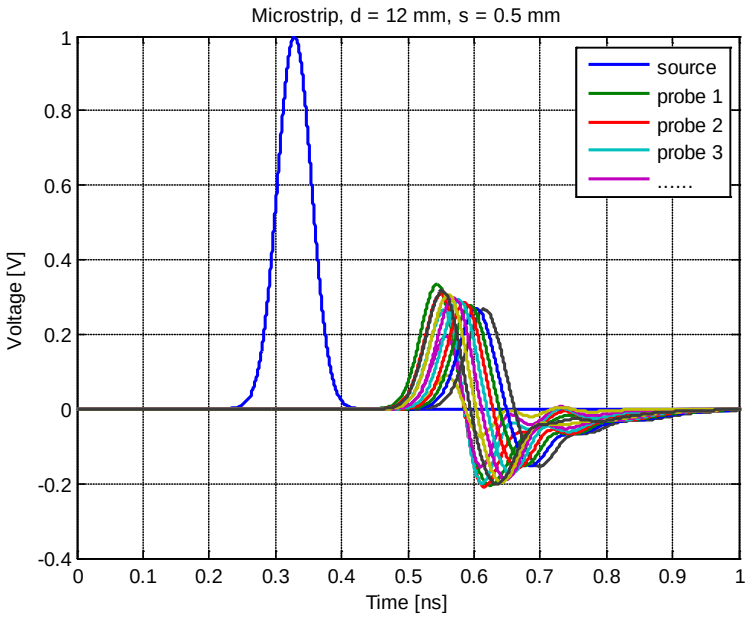

Figure 4.5. Simulation result: voltage waveforms of source and at all the voltage probes.

Figure 4.6 shows the group of impedance curves when $s = 0.5$ mm. The curves have well behaved 20dB/decade linear increment up to several GHz, which can be represented with an inductance. At higher frequency, the capacitance across the split starts to kick in. Furthermore, the lumped circuit model begins to fail as the distributed effect shows up.

Figure 4.7 gives the equivalent inductance calculated from the curves in Figure 4.6. In the lower frequency region with smaller d, the inductance keeps relatively constant. When d is larger, L_e is larger and the capacitance across the split is also more significant. The curve starts to roll off at a lower frequency because more current takes the form of displacement current across the split other than conduction current along the slot and through the shorting tab.

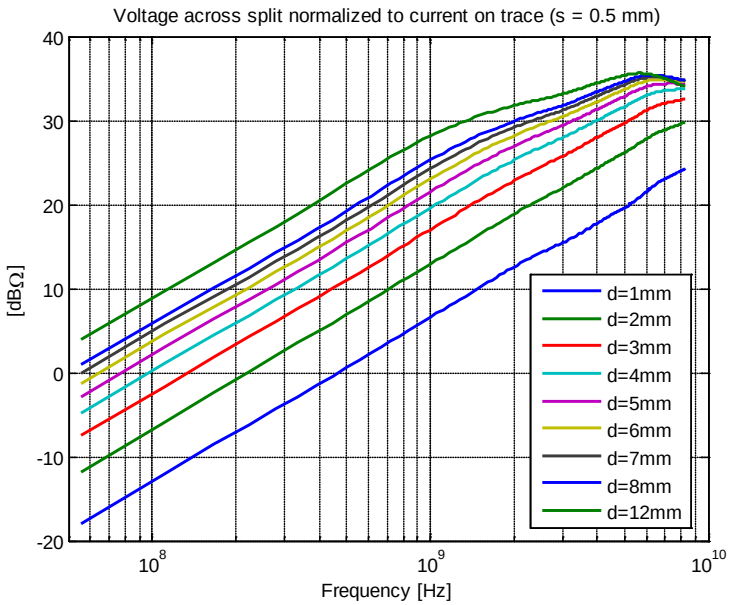

Figure 4.6. Impedance by normalizing maximum voltage across split to current on trace.

Process also the simulation data when $s = 1,\ 1.5\,\text{mm}$. For the low frequency, constant inductance part, the curve fitting function is shown in Equation 4.1. The result is shown in Figure 4.8.

$$L_e = -66 + 6.0(d + 64)^{0.60} - 26e^{-0.53d - 0.098s} + 9.8\log_{10} s \ \text{(dBnH)} \tag{4.1}$$

Where: d is the distance from stitching capacitor to the trace (mm); s is the width of the split (mm).

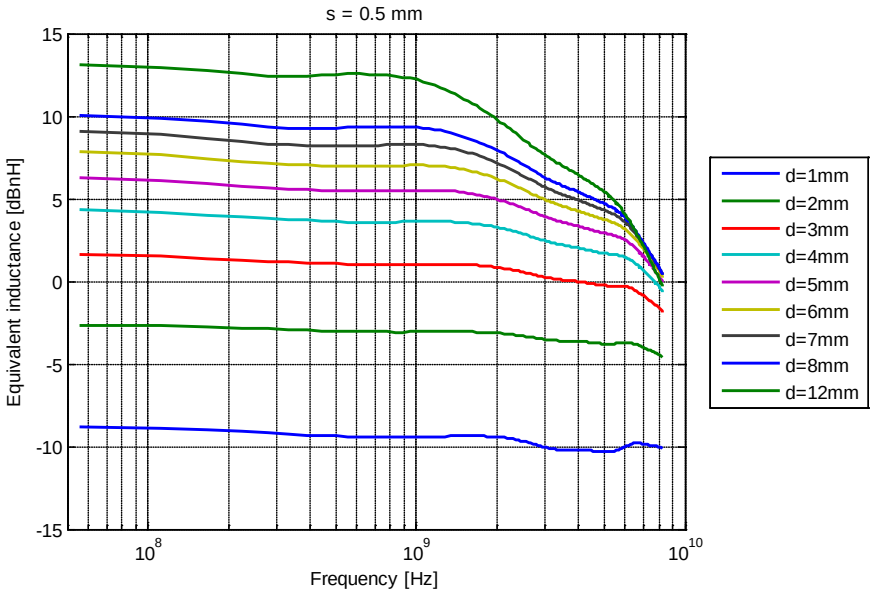

Figure 4.7. Equivalent inductance calculated using the impedance in Figure 4.6.

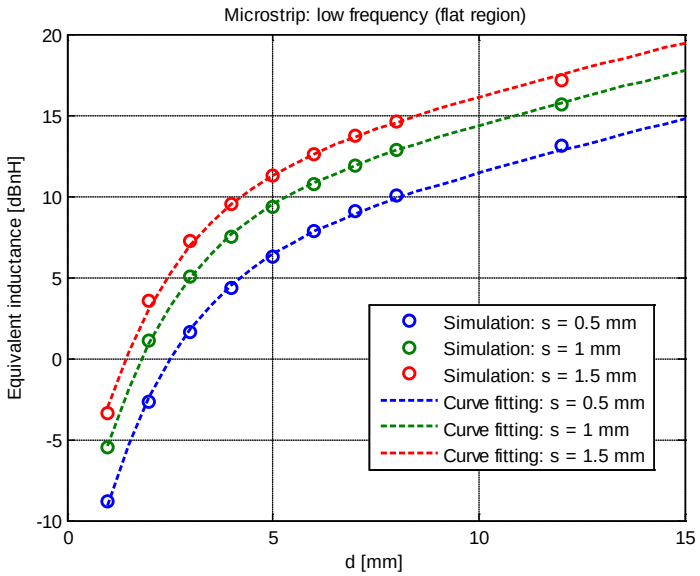

Figure 4.8. Simulation and curve fitting for low frequency part of the equivalent inductance.

4.4. STRIPLINE CROSSING SPLIT PLANES

Stripline across split (Figure 4.9) is another common structure on PCBs. There are four geometry parameters d, s, h_1 and h_2 for calculating the equivalent inductance L_e. But in this case, the ratio of h_2 over h_1 was used instead of using individual h_1 and h_2. This is a reasonable approach as the amount of return current on two reference planes is largely determined by h_2/h_1. The combinations of h_1 and h_2 simulated are shown in Table 4.1. These are common stripline structures often seen on PCBs.

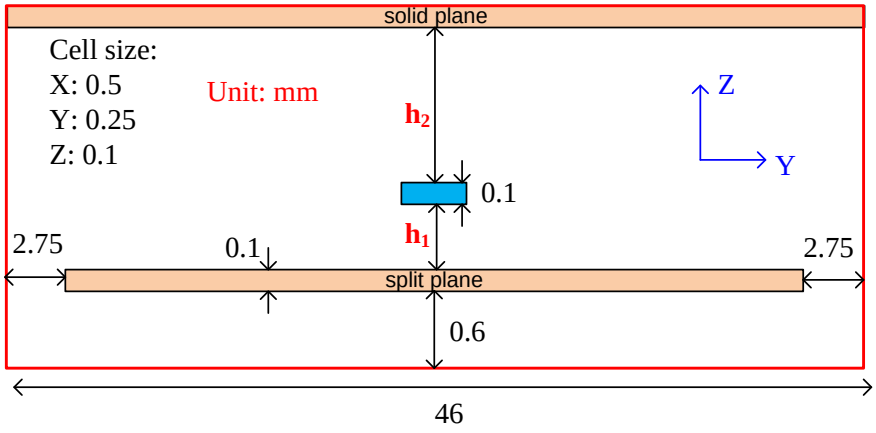

Figure 4.9. Simulation structure of a stripline across split, cross section view.

Table 4.1. Combination of values of $h_1$and h_2 used in simulation.

h_1 (mm)	0.6	0.3	0.3	0.3	0.3
h_2 (mm)	0.3	0.2	0.3	0.4	0.6
h_2/h_1	0.5	0.67	1	1.33	2

The curve fitting function for the low frequency part of the equivalent inductance is shown in Equation 4.2. The simulation data and curve fitting result for the cases when $s = 1\,\text{mm}$ are compared in Figure 4.10. The simulation data when $d = 1,\ 2\,\text{mm}$ were not used for curve fitting because it was dominated by the unwanted current flowing in opposite direction on the two planes. But, this does not matter as the data at very small d can be extrapolated from the curve fitting. Also, it's not usual on a real board for a stitching capacitor to be placed so close to the trace.

$$L_e = 19 - 27d^{-0.28} - 567e^{-9.4k - 0.0015d - 0.022s} + 8.0\log_{10} s + 7.1\log_{10} k \ \ (\text{dBnH}) \qquad (4.2)$$

(To avoid singularity, let $L_e = 0$ nH when $d < 0.1$ mm)

where: $k = h_2 / h_1$; h_1 is the space between split plane and trace (mm); h_2 is the space between solid plane and trace (mm).

4.5. MEASUREMENT VALIDATION

The microstrip configuration simulations were validated by building a test board with microstrip crossing a split, shown in Figure 4.11. Three configurations were measured and modeled in EZ-FDTD simulation: (1) no shorting piece connecting the split (FSV ADMc=4 fair-to-excellent [13]); (2) shorting piece under the trace (in the middle) (FSV ADMc=3 good-to-excellent); (3) shorting piece halfway from trace to board edge(FSV ADMc=3 good-to-excellent). S21 was measured with a vector network analyzer (VNA) for all three cases. The simulation and measurement results are shown in

Figure 4.12 and show good agreement. The FSV ADMc is shown in the insert in Figure 4.12.

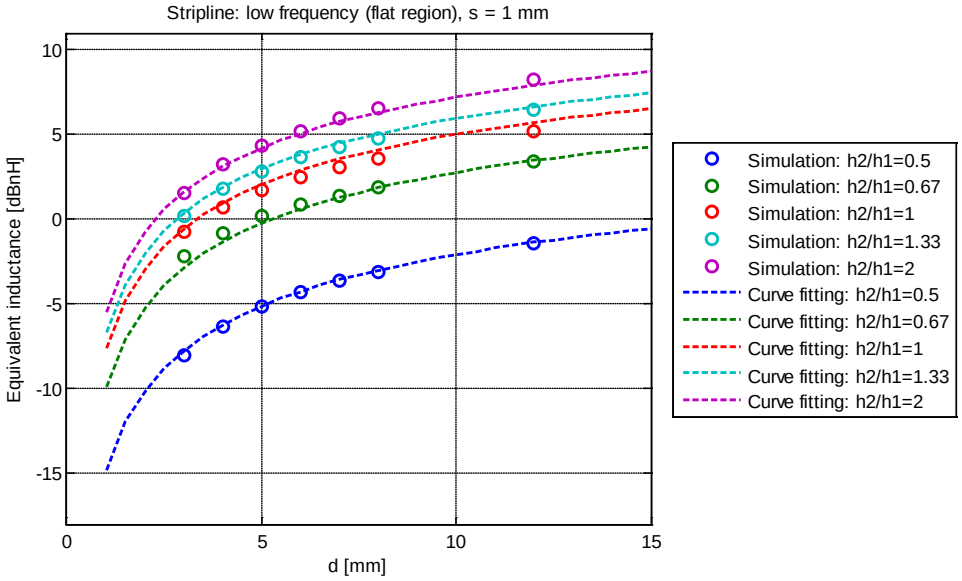

Figure 4.10. Simulation and curve fitting for low frequency part of the equivalent inductance.

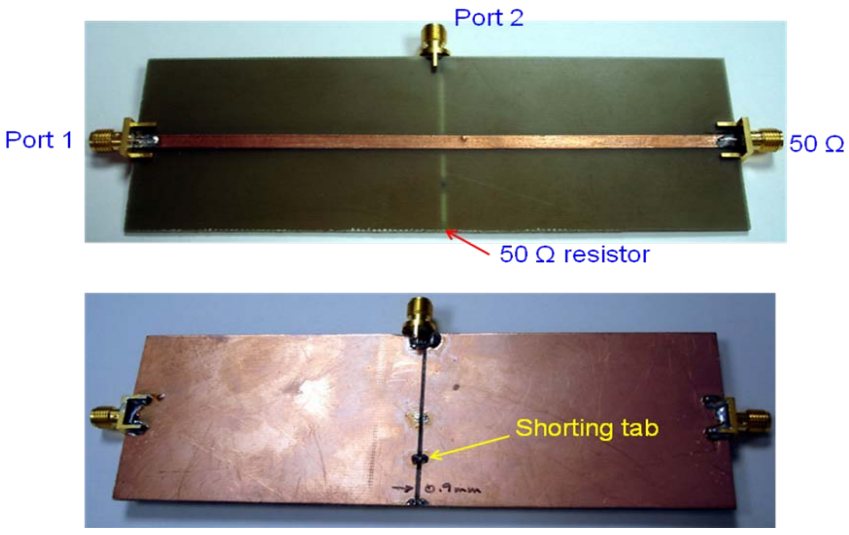

Figure 4.11. Test board with microstrip crossing split.

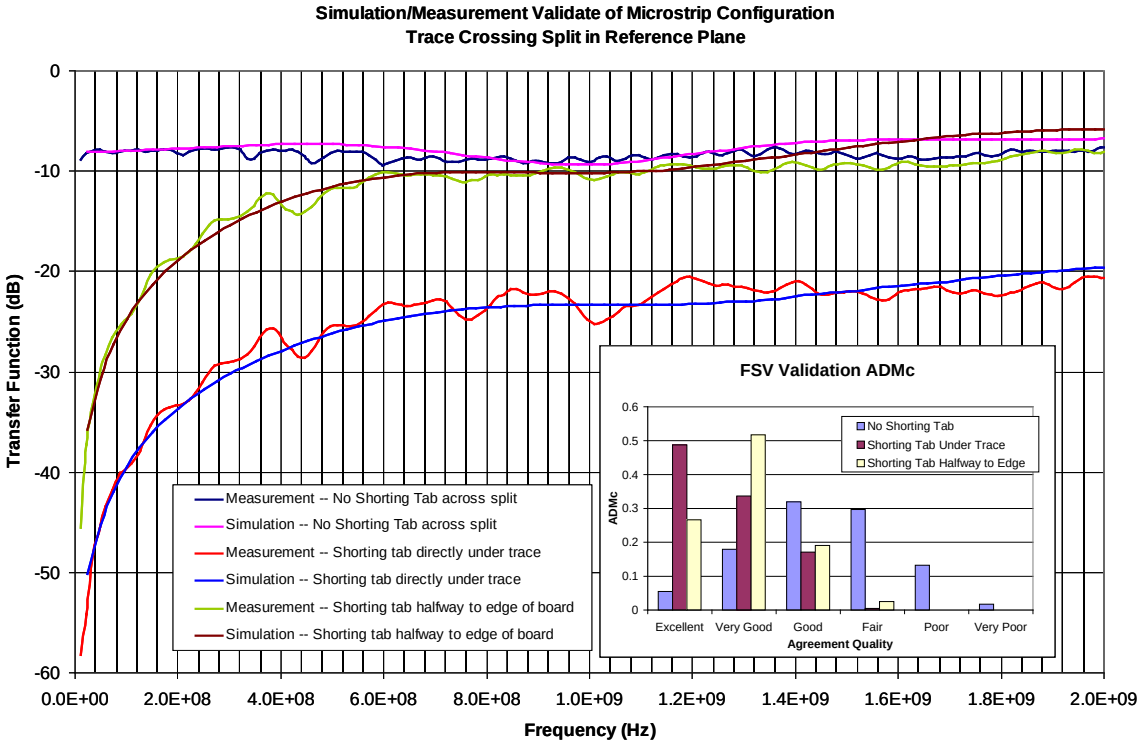

Figure 4.12. Validation between simulation data and measurement result of the test board.

4.6. CONCLUSION

This work has characterized the amount of equivalent inductance on the adjacent split reference plane when return signal current takes the path via a stitching capacitor. Some typical microstrip and stripline configurations were studied. The equivalent inductance can be used together with other parameters (e.g., power plane impedance) of the split planes to quantify the amount of noise voltage seen across a split in the reference plane as a function of harmonic frequency current amplitude, distance to stitching capacitor, split width, and power plane impedances.

REFERENCES

[1] W. Cui, J. Fan, H. Shi, and J. L. Drewniak, “DC power bus noise isolation with power islands,” in Proc. IEEE Int. Symp. Electromagn. Compat., 2001, pp. 899–903.

[2] Archambeault, B.; “Proper design of intentional splits in the ground reference plane of PC boards to minimize emissions on I/O wires and cables,” Electromagnetic Compatibility, 1998. 1998 IEEE International Symposium on Volume 2, 24-28 Aug. 1998 Page(s):768 - 773 vol.2.

[3] Liaw, H.-J.; Merkelo, H.; “Crossing the planes at high speed. Signal integrity issues at split ground and power planes,” Circuits and Devices Magazine, IEEE Volume 13, Issue 6, Nov. 1997 Page(s):22 – 26.

[4] Jingook Kim; Heeseok Lee; Joungho Kim; “Effects on signal integrity and radiated emission by split reference plane on high-speed multilayer printed circuit boards,” Advanced Packaging, IEEE Transactions on Volume 28, Issue 4, Nov. 2005 Page(s):724 – 735.

[5] Chun-Te Wu; Guang-Hwa Shiue; Sheng-Mou Lin; Ruey-Beei Wu; “Composite effects of reflections and ground bounce for signal line through a split power plane,” Advanced Packaging, IEEE Transactions on olume 25, Issue 2, May 2002 Page(s):297 – 301.

[6] Juan Chen; Weimin Shi; Norman, A.J.; Ilavarasan, P.; “Electrical impact of high-speed bus crossing plane split,” Electromagnetic Compatibility, 2002. EMC 2002. IEEE International Symposium on Volume 2, 19-23 Aug. 2002 Page(s):861 - 865 vol.2.

[7] Roden, J.A.; Archambeault, B.; Lyle, R.D.; “Effect of stitching capacitor distance for critical traces crossing split reference planes,” Electromagnetic Compatibility, 2003 IEEE International Symposium on Volume 2, 18-22 Aug. 2003 Page(s):703 - 707 vol.2

[8] IEEE EMC Society Newsletter, Winter 2006 issue, pp 56-67. www.emsc.org

[9] Kim, J.; Kim, H.; Youchul Jeong; Lee, J.; “Slot Transmission Line Model of Interconnections Crossing Split Power/Ground Plane on High-speed Multi-layer Board,” Signal Propagation on Interconnects, 6th IEEE Workshop on. Proceedings 12-15 May 2002 Page(s):23 – 26.

[10] H.W. Johnson and M. Graham, High Speed Digital Design, Englewood Cliffs, NJ: Prentice Hall, 1993

[11] EZ-FDTD Users Manual. www.ems-plus.com, May 2009.

[12] Gisin, F.; Pantic-Tanner, Z.; “Routing differential I/O signals across split ground planes at the connector for EMI control,” Electromagnetic Compatibility, 2000. IEEE International Symposium on Volume 1, 21-25 Aug. 2000 Page(s):325 – 327 vol.1.

[13] Duffy, A.; Martin, A.; Antonini, G.; Orlandi, A.; Ritota, C., "The feature selective validation (FSV) method," Electromagnetic Compatibility, 2005. EMC 2005. 2005 International Symposium on. Volume 1, Issue , 8-12 Aug. 2005.

CONCLUSIONS

This dissertation introduced and categorized various EMI debugging techniques. Experimental examples were provided for the methods. The theoretic foundations were discussed. It also tries to connect some methods by their interrelations. The work presented contributes to the EMC engineering knowledge by evaluating and improving various EMI analysis techniques, testing the methods that worked and failed. One specific type of PCB geometries, trace crossing split planes, was studied to estimate the noise voltage across the slot for EMI evaluation. The curve fitting formulas were developed to calculate equivalent inductance caused by the slot discontinuity. The equivalent inductance is used together with parameters of decoupling and power plane to predict the noise voltage across the slot.

VITA

Weifeng Pan was born on October 20, 1976, in Zhuji, Zhejiang Province, China. He received his BSEE degree in 1999 and MSEE in 2002, both from Tsinghua University, Beijing, China.

In August 2005, he began pursuing Ph.D.'s degree in the Electromagnetic Compatibility Laboratory at Missouri University of Science and Technology. He passed the dissertation defense in May 2009 and received Ph.D.'s degree in August 2009.